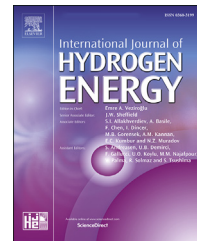


Available online at [www.sciencedirect.com](http://www.sciencedirect.com)**ScienceDirect****ELSEVIER**journal homepage: [www.elsevier.com/locate/he](http://www.elsevier.com/locate/he)

# Design and modular scale-up of shell and tube metal hydride hydrogen storage reactor utilizing multi-pass water flow

Satyaki Chandra <sup>a</sup>, Pratibha Sharma <sup>a</sup>, P. Muthukumar <sup>b</sup>,  
Sankara Sarma V. Tatiparti <sup>a,\*</sup>

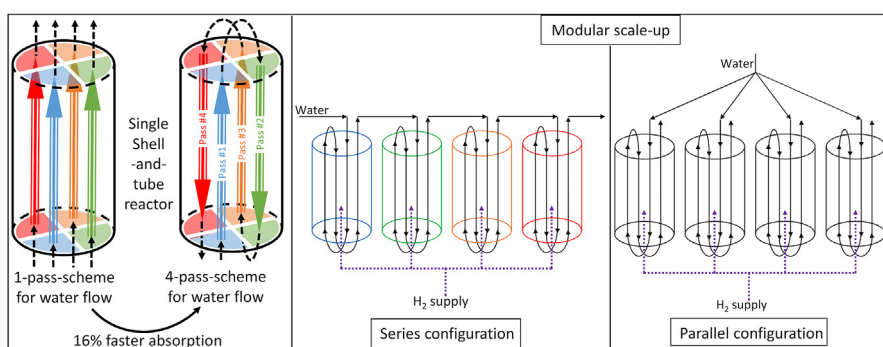
<sup>a</sup> Department of Energy Science & Engineering, Indian Institute of Technology Bombay, Mumbai 400076, India

<sup>b</sup> Department of Mechanical Engineering, Indian Institute of Technology Tirupati, Andhra Pradesh-517619, India

## HIGHLIGHTS

- Shell-and-tube MH reactors are designed and simulated for 1, 4 passes of water flow.
- Trade-off exists between volume occupied by tubes and absorption performance.
- Shell diameter and tube arrangement is varied to find balanced design.
- 4 reactors connected in series or parallel were used together to increase capacity.
- Series performs better at lower flow rates and similarly to parallel at higher.

## GRAPHICAL ABSTRACT



## ARTICLE INFO

### Article history:

Received 9 May 2023

Received in revised form

10 September 2023

Accepted 11 September 2023

Available online 28 September 2023

### Keywords:

Hydrogen storage

Numerical simulation

## ABSTRACT

Shell-and-tube designs with multi-pass fluid flow are not used for metal hydride hydrogen storage reactors. Here, the absorption performances of reactors having shell outer diameter [OD]: 114.3, 141.3 and 168.3 mm with 36, 60 and 92 tubes arranged in 3, 4 and 5 circular arrays housing 25 kg LaNi<sub>5</sub> at 20 bar hydrogen pressure, 10 LPM water entering at 30 °C are simulated. Considering the trade-off between tube volume and reaction duration, OD: 141.3 mm, 60 tubes offers a balanced performance with 90% absorption taking ~320 s with four water passes (4-pass-scheme) vis-à-vis ~380 s with one pass (1-pass-scheme). This design is scaled-up to house 100 kg LaNi<sub>5</sub> with four modules in series and parallel configurations. When in series, reactors take 320, 425, 545, and 665 s for 90% absorption; in

\* Corresponding author.

E-mail address: [sankara@iitb.ac.in](mailto:sankara@iitb.ac.in) (S.S.V. Tatiparti).

<https://doi.org/10.1016/j.ijhydene.2023.09.128>

0360-3199/© 2023 Hydrogen Energy Publications LLC. Published by Elsevier Ltd. All rights reserved.

Shell and tube  
Multi pass flow  
Scale up  
LaNi<sub>5</sub>

parallel, each reactor takes 625 s. At higher water flow rate (40 LPM) series and parallel configurations perform similarly.

© 2023 Hydrogen Energy Publications LLC. Published by Elsevier Ltd. All rights reserved.

Nomenclature			Greek symbols Description	
Symbols	Description	Unit	$\epsilon$	Porosity
C	Rate constant		$\kappa$	Permeability m <sup>2</sup>
c <sub>p</sub>	Specific heat at constant pressure	J kg <sup>-1</sup> °C <sup>-1</sup>	$\mu$	Viscosity Pa s
E	Activation energy	J (mol H <sub>2</sub> ) <sup>-1</sup>	$\rho$	Density kg m <sup>-3</sup>
h	Convective heat transfer coefficient	W m <sup>-2</sup> °C <sup>-1</sup>		
(H/M)	Hydrogen atom absorbed per atom of metal hydride			
$\Delta H$	Enthalpy of metal hydride formation	J (mol H <sub>2</sub> ) <sup>-1</sup>		
ID	Inner diameter	mm		
OD	Outer diameter	mm		
k	Thermal conductivity	W m <sup>-1</sup> °C <sup>-1</sup>		
M	Molar mass	kg mol <sup>-1</sup>		
m	mass	kg		
P	Pressure	bar		
Q	Heat	J		
R <sub>u</sub>	Universal gas constant	J mol <sup>-1</sup> °C <sup>-1</sup>		
$\Delta S$	Entropy of metal hydride formation	J (mol H <sub>2</sub> ) <sup>-1</sup> °C <sup>-1</sup>		
T	Temperature	°C		
t	Time	s		
v	Velocity	m s <sup>-1</sup>		
V	Volume flow rate	LPM or L min <sup>-1</sup>		
wt%	Weight percentage of hydrogen within metal hydride			
X	Reacted fraction			
Subscripts			Description	
abs	Absorption process			
amb	Ambient			
eff	Effective			
eq	Equilibrium			
gen	Generation			
H2	Hydrogen gas			
i	Inlet			
mass	Mass			
MH	Metal hydride at any time instance			
o	Outlet			
ref	Reference			
s	Supply			
sat	Saturation			
t	At a particular time instance			
tube	Tube			
w	Water			
1-pass	1-pass-scheme of water flow			
4-pass	4-pass-scheme of water flow			

## 1. Introduction

Hydrogen is a promising green-fuel because it has a high energy density of 140.4 MJ kg<sup>-1</sup> [1] and can be generated by renewable means like photo-catalytic water splitting [2], biomass [3] etc. Generation of electricity and mechanical work from hydrogen is possible through fuel cells [4–7] and H<sub>2</sub> IC engines [7–9], respectively. The exhaust from these devices is mostly water vapor. The conventional storage of hydrogen is by compressing it to 350–700 bar, which owing to high pressures can prove risky. Liquefaction of hydrogen needs cryogenic temperatures, which is not cost effective and involves losses. Alternatively, hydrogen can be stored in solid hosts like metal hydrides (MH) based on LaNi<sub>5</sub> [10–15], FeTi [16–18], Mg [19–22] etc. LaNi<sub>5</sub> can store hydrogen at near-ambient pressures and temperatures. Typically, MH is used as a porous bed. As the porous MH beds are poor conductors of heat and the exothermic absorption and the endothermic desorption process requires the inclusion of a heat transfer system (HTS) [23,24].

Various HTS designs are reported in literature with a heat transfer fluid (HTF) to transfer the heat from/to the MH bed. Water is a widely used HTF because of its high heat capacity and availability. Askri et al. [25] and Kaplan [26] compared several designs with water and air as HTFs. Water was able to remove heat at a faster rate and thus was able to accelerate the absorption process. This reduces the total duration of the process, which is desirable. There are several recent literature where the authors are combining the MH reactor with thermal storage using phase change material (PCM) [27–31]. Such a design have the opportunity to contain the generated heat during the absorption process but loses the cooling potential as the PCM gets hotter. As our motivation is to study a reactor which improves the kinetics of the absorption reaction by providing a superior cooling. Thus, a water cooled design will be adapted for the current design. The design of the HTS plays an important role as it is the heat transfer medium between the MH bed and the HTF. Researchers have been investigating on various HTS designs to enhance the heat transfer. Muthukumar et al. [32] proposed a cost-effective design of a shell and tube type storage reactor entirely made of SS316.

Their reactor shell of internal diameter (ID): 50 mm contained 12–20 tubes and a central metal filter for hydrogen supply to the MH bed of  $\text{MmNi}_{4.6}\text{Al}_{0.4}$ . With the assumption of  $U: 1000 \text{ W m}^{-2} \text{ K}^{-1}$  for HTS carrying water at  $30^\circ\text{C}$ , the absorption performance improvement was observed by increasing the numbers of tubes. In an experimental study by the same group, Anbarasu et al. [33] demonstrated that an improvement of absorption performance is possible by using a higher number of tubes, higher pressure, lower water temperature and higher flow rate using two shell and tube type reactors with 36 and 60 tubes, each containing 2.75 kg of  $\text{LmNi}_{4.91}\text{Sn}_{0.15}$  (Lm: La-based misch material). Under hydrogen supply pressure ( $P_{\text{H}_2,\text{s}}$ ): 25 bar, water velocity ( $v_w$ ):  $0.33 \text{ m s}^{-1}$  and water inlet temperature ( $T_{w,i}$ ):  $30^\circ\text{C}$ , absorption took 25% shorter time for the reactor with 60 tubes compared to that with 36 tubes. Raju et al. [34] and Kumar et al. [35] used shell (outer diameter (OD): 114.3 mm, ID: 102.26 mm) and tube (55) reactors with  $\text{LaNi}_{4.7}\text{Al}_{0.3}$  [34] and  $\text{MmNi}_{4.7}\text{Fe}_{0.3}$  [35], respectively. Kumar et al. [36] eventually designed a scaled-up version of their reactor by including 99 HTS tubes. This reactor has a capacity of 40 kg  $\text{LaNi}_{4.7}\text{Al}_{0.3}$  and could store 552 g of hydrogen in  $\sim 300$  s under  $P_{\text{H}_2,\text{s}}$ : 40 bar, water flow rate ( $V_w$ ): 30 LPM and  $T_{w,i}$ :  $30^\circ\text{C}$ . A set of design guidelines along with several performance comparisons of similar shell and tube reactors was presented by Raju and co-workers [37]. The designs were with 114.30 mm shell OD + 40 tubes, 141.30 mm shell OD + 67 tubes, 168.28 mm shell OD + 99 tubes, and 219.08 mm shell OD + 136 tubes and took 1150, 813, 685, and 813 s, respectively at  $P_{\text{H}_2,\text{s}}$ : 30 bar,  $V_w$ : 60 LPM and  $T_w$ :  $30^\circ\text{C}$  to absorb  $\sim 1.2$  wt% of hydrogen [37]. Interestingly, Gkanas et al. [38] presented a rectangular reactor (shell) design, which is a deviation from the conventional circular counterparts. They discussed the effects of various numbers of equally spaced tubes, different tank dimensions with  $\text{LaNi}_5$ ,  $\text{MmNi}_{4.6}\text{Al}_{0.4}$  and a novel AB<sub>2</sub> material (undisclosed) as the storage host MH [38]. Liu et al. [39] also investigated the effect of tube arrangement on the sorption performance of shell-and-tube type reactor. Recently, Pandey et al. [40] used a common water jacket of 350 mm ID which enclosed 7, 14 and 19 tubes of different diameter containing MH. Higher number of tubes with better contact with water resulted in faster absorption viz. 90% absorption in 985, 404, and 317 s, respectively for  $P_{\text{H}_2,\text{s}}$ : 15 bar and  $T_{w,i}$ :  $25^\circ\text{C}$  [40]. Pandey et al. [40] also discussed the effect of various number of internal fins on the inner walls of the aforementioned tubes, which improves the performance further. A reactor with seven tubes holding a total of 50 kg  $\text{LaNi}_5$  surrounded by a common water jacket was conceptualized by Afzal et al. [41] numerically, was fabricated and experimentally studied by Gupta et al. [42]. In another recent work, Aadithiyan et al. [43] explored various design approaches for reactors with 2.75 kg of  $\text{LmNi}_{4.91}\text{Sn}_{0.15}$  hydride capacity. They compared various designs of embedded cooling tubes, capillary and tubular bundled reactors, helical coiled reactors and proposed suitable designs for desirable sizing and performance [43]. Another recent comparative study by Sreeraj et al. [44] focuses on (i) shell and tube, (ii) spiral tube, and (iii) tubular reactors each with 5 kg  $\text{LaNi}_5$  capacity. A spiral tube reactor with three such tubes is an optimal design from the view point of sorption performance and capacity. The authors proposed to attach heat pipes to the

same for further enhancement of performance [44]. The increase in contact area between MH bed and heat transfer surface plays a much important role in cooling and making the absorption faster which is evident from the literature so far. Some recent literatures used innovative and relatively complicated fins for this purpose [45–48]; whereas a design with tube-like channels with rectangular cross-section arranged  $60^\circ$  apart was suggested by Bai et al. [49] in their recent work. This design can result in a much higher surface contact than the design with circular cross-section of regular tubes. The recent work of Eisapour et al. [50] shows the use of helical tubes with a central return tube in a cylindrical  $\text{Mg}_2\text{Ni}$  bed. Eisapour et al. [50] observed a more uniform distribution of temperature due to the inclusion of this central return tube that makes the process 24% faster. Tiwari et al. [51] optimized various design parameter for a cylindrical  $\text{Mg}_2\text{Ni}$  reactor with helical cooling coil to maximize water outlet temperature and/or reacted fraction. A set of experimental results under various operating parameter for a reactor with 640 g of  $\text{LaNi}_5$  and helical coil was presented by Bao et al. [52] Wang et al. [53] in their recent study proposed the use of various arrangements of helical tubes with elliptical cross-section rather than the conventional circular one. This can provide even higher surface contact area [53]. Another design from the same authors utilized radial branch-like mini-channels connected with longitudinal tubes for a much uniform distribution of temperature and reacted fraction throughout the MH bed resulting in faster reaction [54].

Most of the efforts in literature on hydrogen storage in metal hydride reactors focus on single pass scenarios involving unidirectional flow of HTF. Multi pass schemes are more common in fluid-to-fluid heat exchangers with shell-and-tube design. These schemes are known for their better heat exchange and can be economical. However, multi pass schemes are not explored extensively in the context of hydrogen storage in a metal hydride, where heat exchange happens across hydrogen gas (fluid) and metal hydride (solid). This is possibly because the existing efforts in literature focus mainly on improving the heat transfer effect by improving the design of the heat transfer system. Nevertheless, very few reports exist on the use of more than one pass of HTF flow. For example, Singh et al. [55] used two SS U-tubes attached with 13 perforated copper fins in their reactor with 1 kg  $\text{LaNi}_5$  along with 80 g of copper flakes. In the numerical part of this study, they simulated the positive effect of higher number of thinner fins and higher diameter of the U-tubes [56]. Lewis et al. [57] used four U-tubes to enhance the performance in their reactor with and without fins. The numerical optimization and experiments by Visaria et al. [58,59] involves SS U-tubes fitted with SS fins and the operating pressure was chosen to be variable for a faster absorption process. The utilization of U-tubes for hydrogen storage, mentioned above, possesses the advantage of two passes. For a better understanding of the effect of multi pass the results of the same should be compared with those from single pass within the same reactors. Moreover, efforts tuned towards scaling up of multi pass schemes should be carried out. Hence, the novelty of this work is to explore the effect of multi pass scheme of HTF (water) flow on heat exchange in shell-and-tube type metal hydride reactors during hydrogen storage. Eventually, the

scale-up of the multi-pass scheme through modular approach where several reactors connected in series and parallel configurations is also explored.

For a fixed volume flow rate a multi-pass scheme results in a higher water velocity than a single-pass scheme. This results in higher heat transfer coefficient in multi-pass scheme. On the other hand, as the water exits from one pass and enters the next, its inlet temperature is higher for the later passes. Thus, the latter passes remove heat only less effectively than the former ones. An important question here is: What is the combined effect of these two opposing parameters i.e. higher heat transfer coefficient and higher inlet temperature in the latter passes? This question is answered by making a few modifications to our shell-and-tube reactor design from the literature survey presented above. Some designs used different number of tubes arranged in circular arrays and varied the number of arrays along with the tube spacing to achieve different designs [60]. Raju et al. [37] fixed the tube spacing and then calculated the tube arrangement for different number of tubes and shell diameters. Other researchers looked into the arrangement of the tubes [38]. In the present work the tubes are arranged in a few circular arrays inside a cylindrical shell, where each of these arrays consists of  $4n$  number of tubes ( $n$ : any integer) to facilitate four passes of HTF. Shells with ODs of 114.3, 141.3, 168.3 mm containing 36, 60 and 92 tubes, to contain 25 kg of LaNi<sub>5</sub> in each reactor are considered in this work. Designs containing more than four passes are not considered as they can be complicated. The designs considered in this study are used for comparison between the performances (time taken for 90% absorption) of one pass and four passes viz. 1-pass-scheme and 4-pass-scheme of HTF flow under the same operating conditions ( $P_{H2,s}$ : 20 bar,  $V_w$ : 10 LPM, and  $T_{w,i}$ : 30 °C). The results show that the 4-pass-scheme offers better performance than the 1-pass-scheme in the present conditions.

Scale-up is necessary in hydrogen storage for practically maximizing the hydrogen capacity. The optimized design from the above mentioned ones is used, further, for modularly scaling up by connecting four reactors in both series and parallel combinations (separately) with HTF to contain 100 kg of LaNi<sub>5</sub>. The results of this scale up exercise show that at lower flow rate (10 LPM) the series combination offers faster absorption. At higher water flow rate (40 LPM) both these configurations perform similarly.

## 2. Reactor design

The reactors considered in the present study possess shell made of commercially available SS316 standard tubes (Sch-40s). Three shell diameters: 114.3, 141.3 and 168.3 mm are considered here. This is to facilitate the possibility of immediate procurement of these shells with standard diameters and construct the reactors. Continuous variation of shell diameter for its optimization is not attempted here. This is because if the optimized diameter is a non-standard one then fabricating it would incur additional cost and time. Moreover, continuous variation of shell diameter may necessitate the use and optimization of a different thermal management system inside the reactors. The authors used the diameters of

Sch-40s in their previous simulation and experimental studies [61–63] and demonstrated promising hydrogen absorption/desorption and scaled-up performance by LaNi<sub>5</sub> in these reactors. Fig. 1a shows an example of the tube arrangement of a reactor with the shell of 141.3 mm OD and 6.02 mm thickness. There are 60 HTS tubes arranged in four circular arrays in this design. The arrangement of tubes ensures that they can be divided in four zones as shown in Fig. 1a to facilitate four

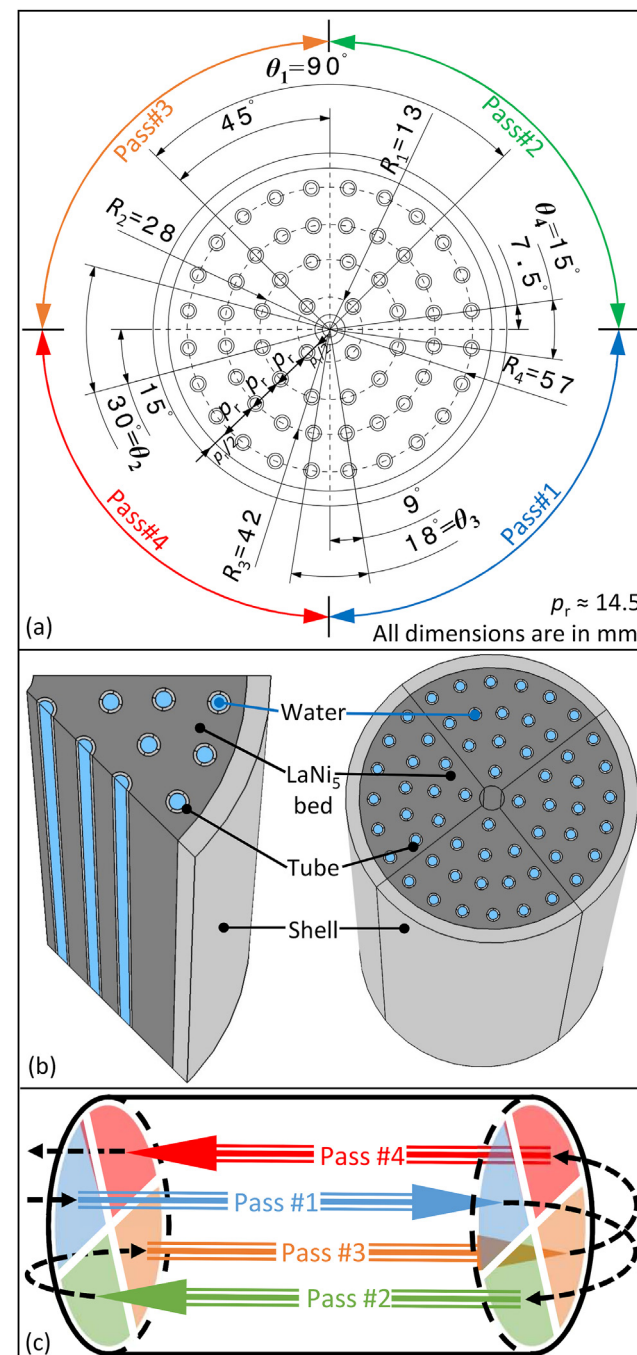


**Fig. 1 – Shell-and-tube type 25 kg LaNi<sub>5</sub> based hydrogen storage reactor:** (a) Cross section of Shell 141.3 mm - 60 Tubes design, (b) domains in 1/8th section and full section showing various components, (c) water flow directions in 4-pass-scheme.

passes of water flow. A similar arrangement of tubes is adapted for the other designs. The shell contains 25 kg LaNi<sub>5</sub> (i.e. metal hydride, MH) bed along with an HTS (heat transfer system) consisting of tubes with diameter 0.25" (6.35 mm) and made of SS316. The tubes are arranged perimetrically (i.e. in circular arrays) around the axis of the reactor shell. The radial distance between any two adjacent circular arrays is equal and denoted as  $p_r$ . The center of any tube in the innermost circular array is radially  $p_r/2$  away from the outer surface of the centrally located sintered SS316 filter. This filter is 12 mm in OD and acts as a hydrogen artery that ensures uniform distribution of hydrogen gas along the length of the MH bed contained inside the reactor shell. The radial distance between the center of any tube located in the outermost circular array and the inner surface of the reactor shell is maintained as  $p_r/2$  using Eq. (1).

$$p_r = \frac{r_{\text{shell}} - R_{\text{filter}}}{n_{\text{array}}} \quad (1)$$

The distance between any two adjacent tubes of  $j$ th array (radius:  $R_j$ ) as  $p_r$  by using Eq. (2), where  $\theta'_j$  is the angular separation between these tubes (Fig. 1a).

$$\theta'_j = 2 \cdot \sin^{-1} \left( \frac{p_r}{2R_j} \right) \cdot \frac{360^\circ}{2\pi} \quad (2)$$

The number of tubes in  $j$ th array is calculated by dividing  $360^\circ$  by  $\theta'_j$ . This number can be a non-integer value, through this calculation. Hence, it is adjusted (denoted as  $n_j$ ) to an integer divisible by 4 to realize the possibility of four passes. Consequently,

$$\theta_j = \frac{360^\circ}{n_j} \quad (3)$$

Various dimensions of the components used in different designs (and their names) employed in the present study along with the calculated values of  $\theta_j$  are shown in Tables 1 and 2. From these tables, the value of  $p_r$  changes with each design according the number of circular array and shell diameter.

### 3. Numerical simulation

#### 3.1. Computational domains

The model was created using COMSOL 5.4 and has several domains on which simulations are run using finite element method. Fig. 1b shows various computational domains viz. LaNi<sub>5</sub> porous bed, water (HTF), SS316 shell wall and tube. The properties of LaNi<sub>5</sub> bed are listed in Table 3. To simulate 1-pass-scheme through all the HTS tubes (i.e. water flowing in one direction), a 1/8th longitudinal section is used to reduce the computational load. For 4-pass-scheme, the whole reactor model is used. The four passes in this scheme are named as Pass#1, 2, 3 and 4, dedicated to the respective zones (indicated by four different colors) as shown in Fig. 1c. The central metal filter, the top and bottom flanges are not modeled as they exercise little influence on heat transfer compared to that of the HTS.

**Table 1 – Designs considered to test the effect of distance between tubes for a constant shell diameter.**

	Shell OD (mm)	Shell Thickness (mm)	Number of circular arrays	Calculated radial distance, $p_r$ (mm)	Array number	Radial distance of shell from axis (mm)	Calculated radial pitch, $\theta'_j$	Used radial pitch, $\theta_j$	Used number of tubes	Liner axis-to-axis distance (mm)	Total number of tubes	Bed height, L (mm)
Shell141.3 mm-36Tubes	141.3	6.55	3	19.37	Array # 1	16	64.99°	90°	4	22.63	36	517
					Array # 2	35	30.07°	30°	12	18.12		
					Array # 3	54	19.69°	18°	20	16.89		
Shell141.3 mm-60Tubes	141.3	6.55	4	14.53	Array # 1	13	67.93°	90°	4	18.38	60	553
					Array # 2	28	30.07°	30°	12	14.49		
					Array # 3	42	19.91°	18°	20	13.14		
					Array # 4	57	14.64°	15°	24	14.88		
					Array # 1	12	66.25°	90°	4	16.97		
					Array # 2	23	30.51°	30°	12	11.91		
					Array # 3	35	19.48°	18°	20	10.95		
					Array # 4	47	14.58°	15°	24	12.27		
					Array # 5	58	11.65°	11.25°	32	11.37		

Table 2 – Designs considered to test the effect of shell diameter for almost same distance between tubes.							
	Shell OD (mm)	Shell Thickness (mm)	Number of circular arrays	Calculated radial distance, $p_r$ (mm)	Array number	Radial distance of from shell axis (mm)	Calculated radial pitch, $\theta_j'$
Shell114.3 mm-36Tubes	114.3	6.02	3	15.04	Array # 1 Array # 2 Array # 3 Array # 1 Array # 2 Array # 3 Array # 4 Array # 1 Array # 2 Array # 3 Array # 4 Array # 5	14 29 44 13 28 42 57 13 27 42 56 70	64.9° 30.07° 19.69° 67.93° 30.07° 19.91° 14.64° 66.25° 30.51° 19.48° 14.58° 11.65°
Shell141.3 mm-60Tubes	141.3	6.55	4	14.53	14.21	14.21	
Shell168.3 mm-92Tubes	168.3	7.11	5				

Table 3 – Properties of LaNi<sub>5</sub> [56,61–63,66,74,75].

Name	Symbol	Value	Unit
Activation energy for absorption reaction	$E_{\text{abs}}$	21179.6	J (mol H <sub>2</sub> ) <sup>-1</sup>
Reaction rate constant	$C_{\text{abs}}$	59.187	s <sup>-1</sup>
Crystal density of when unsaturated	$\rho_{\text{MH}}$	8300	kg m <sup>-3</sup>
Weight fraction of maximum absorbed hydrogen	wt% <sub>sat</sub>	1.4%	
Crystal density at saturation	$\rho_{\text{MH,sat}}$	8416.2	kg m <sup>-3</sup>
Enthalpy of formation	$\Delta H_{\text{abs}}$	30800	J (mol H <sub>2</sub> ) <sup>-1</sup>
Entropy of formation	$\Delta S_{\text{abs}}$	108	J (mol H <sub>2</sub> ) <sup>-1</sup> °C <sup>-1</sup>
Molar mass	$M_{\text{MH}}$	0.432	kg mol <sup>-1</sup>
Universal gas constant	$R_u$	8.314	J mol <sup>-1</sup> °C <sup>-1</sup>
Porosity of bed	$\epsilon$	0.5	
Permeability of bed	$\kappa$	10 <sup>-8</sup>	m <sup>2</sup>
Slope factor	$\varphi$	0.038	
$\varphi_0$		0	
Hysteresis factor	$\beta$	0.137	
Thermal conductivity	$k_{\text{MH}}$	2.4	W m <sup>-1</sup> °C <sup>-1</sup>
Heat capacity	$c_{p,\text{MH}}$	419	J kg <sup>-1</sup> °C <sup>-1</sup>

### 3.2. Assumptions

To make the simulations computationally less expensive while preserving the accuracy of the results, the following assumptions are made in the present study [25,32,56,61–66].

- The pressure and temperature ranges for this study are much higher than their values at critical point of hydrogen gas. Hence, hydrogen is considered to behave like an ideal gas.
- The chemical reaction for hydrogen absorption is LaNi<sub>5</sub> + 3H<sub>2</sub> → LaNi<sub>5</sub>H<sub>6</sub> (~1.4 wt%, see Table 3).
- The thermo-physical properties, porosity and volume of the MH bed do not vary with temperature, pressure and concentration of hydrogen absorbed.
- The gas remains in thermal equilibrium with the immobile porous solids locally.
- The dominant mode of heat interaction is conduction in this context. Hence, only conduction is considered here with an effective thermal conductivity of MH material.

### 3.3. Problem definition

Hydrogen gas flows through the porous immobile MH bed and reacts with it exothermically. The governing mass, energy and momentum equations are mentioned in “Supplementary Information” and were also used in our previous works [61–63]. These governing equations along with the HTF water flow through the tubes are solved with the boundary and initial condition mentioned in the next sub-section.

### 3.4. Initial and boundary conditions

Initially the MH bed, water, shell and tubes are at a temperature of  $T = T_{w,i}$  (water inlet temperature). LaNi<sub>5</sub>-bed domain initially has zero reacted fraction,  $X = 0$ . Hydrogen has zero initial velocity,  $v_{H2} = 0$  and is at a pressure of  $P_{H2} = P_{H2,s}$  (supply pressure).

The water and tube domain interface have no slip conditions. The inner boundary of MH domain where the hydrogen enters from the filter, the pressure boundary condition (B.C.)  $P_{H2} = P_{H2,s}$  is assigned. The outer wall of the shell rejects heat to the atmosphere which is much less than the heat removal by water. Hence, an insulated B.C. is considered at the outer wall of the shell.

The 1-pass-scheme has  $T = T_{w,i}$  as the temperature B.C. at the inlets of the water domains located in one end of the reactor. The velocity B.C. in the aforementioned boundaries is defined with fully developed flow with velocity  $v_{w,1\text{-pass}}$ .

$$v_{w,1\text{-pass}} = \frac{V_s}{n_{\text{tube}} \cdot \frac{\pi}{4} \cdot ID_{\text{tube}}^2} \quad (4)$$

All the inlet and outlet B.C.s for water domains belonging to a particular zone are the same (Fig. 1c). Also the inlet temperature of the zone with higher number is the same as the outlet temperature of that with the immediate lower number, i.e.  $T_{w,i,\#m+1} = T_{w,o,\#m}$  ( $m = 1, 2$  and  $3$ ). However, for the first zone  $T_{w,i,\#1} = T_{w,i}$ . The condition of fully developed flow is used for the velocity inlet B.C. of water, i.e.  $v_{w,4\text{-pass}}$  as shown in Eq. (5).

$$v_{w,4\text{-pass}} = \frac{V_s}{n_{\text{tube}} \cdot \frac{\pi}{4} \cdot ID_{\text{tube}}^2} \quad (5)$$

### 3.5. Numerical modelling

To solve the governing equations mentioned in the Supplementary Information using the above mentioned boundary and initial conditions, we used the commercially available finite element based software tool COMSOL Multiphysics 5.4. Physics modules such as laminar flow used for water flow, Darcy's law for hydrogen flow through the porous media, heat transfer in solids (fins), fluid (water) and porous media (hydrogen and LaNi<sub>5</sub>-bed) are solved in tandem. To reach the solutions, the segregated approach using the direct solver PARDISO was adapted. The time dependent solver has different time steps ( $\Delta t$ ) for different time ( $t$ ) ranges viz.  $\Delta t: 0.5$  s for  $t: 0\text{--}50$  s,  $\Delta t: 5$  s for  $t: 50\text{--}1000$  s and  $\Delta t: 25$  s for  $t: 1000$  s till end. Such combination of time steps helps in capturing the initial sharp variation in temperature and reacted fraction and also facilitates a relatively quicker solution with larger  $\Delta t$  values for the later stages of the process where changes in absorbed quantity of hydrogen and temperature are much smaller. The settings and coupling of various physics modules in COMSOL software are schematically represented in "Multiphysics setup in COMSOL" section in Supplementary Information. The coupling of various equations in physics modules was done by using the different physic modules given in "Governing equations" section in Supplementary Information. Also, the input values used for various parameters in these physics modules are listed in Table 3 of the revised manuscript.

### 3.6. Grid independency test and validation

A 1/8th longitudinal section of the design namely Shell141.3 mm-60Tubes (Table 2) is used for checking the grid independency. Three meshing schemes with coarse, normal and fine meshes are generated with the inbuilt meshing tool with 3800, 7130 and 14910 prism elements, respectively, for this design and shown in Fig. 2a. The reason for using prism elements with their length along that of the reactor is: (i) water flow direction is along the length, (ii) variation of water velocity and temperature of all the domains have higher slopes in the radial and angular directions than in the longitudinal direction, (iii) the variation of reacted fraction follows the temperature variation, closely. The average bed and water outlet temperatures ( $T_{\text{bed}}$  and  $T_{w,o}$ ); and the average reacted fraction ( $X$ ) for the aforementioned design with the three grid settings are shown in Fig. 2b and c, respectively. The results generated by normal mesh setting almost overlap with those generated by using fine mesh setting, which have twice the number of grids. Hence, the rest of the study is conducted using the normal mesh setting.

To validate the model, experimental results from two reported studies are chosen. The study by Anbarasu et al. [33] features a shell and tube design with 60 cooling tubes and LmNi<sub>4.91</sub>Sn<sub>0.15</sub> as metal hydride. The properties of this material are documented in their other studies [43,60]. The work of Karmakar et al. [67] uses LaNi<sub>5</sub> as the storage medium and features water jacket along with four tubes carrying water. Both of these designs use SS316. The designs are recreated and various operating parameters and properties are used as input. The results are generated using the normal mesh setting mentioned above. The obtained simulated results in this study show good agreement with experimental results reported in their works as shown in Fig. 3.

## 4. Results and discussion

For all the reactor designs considered here, the same hydrogen supply pressure  $P_{H2,s}$  of 20 bar is used to facilitate comparison of the present results with those from literature. Water supply temperature ( $T_{w,i}$ ) is fixed at 30 °C - close to ambient temperature of the authors' region. Water acts as the heat transfer fluid (HTF) and gets hotter as it flows through the tubes, due to the exothermic nature of hydrogen absorption. The performance of 1-pass-scheme and 4-pass-scheme for all the designs are checked with the same total water flow rates ( $V_w$ ) of 10 and 40 LPM to prevent its boiling. Moreover, the bed porosity is fixed at 0.5 for all the cases (See Table 3) to maintain consistency with the other published works from literature [40,44,53,55,56,65,68,69].

The absorption process for 1-pass water flow scheme through a design namely 'Shell141.3 mm-60Tubes' is described in detail here. The design parameters of this design can be found in Table 1. Fig. 4a consists of the time dependent variation of the average of the bed temperature ( $T_{\text{bed}}$ ) and average value of reacted fraction ( $X$ ). At the very beginning of the absorption process, the reaction is driven at a rapid rate (see "Reacted fraction,  $X''$ , Fig. 4a) due to a high value of the ratio of  $P_{H2,s}$  and the equilibrium pressure,  $P_{\text{eq}}$  (from Eq. S4 in

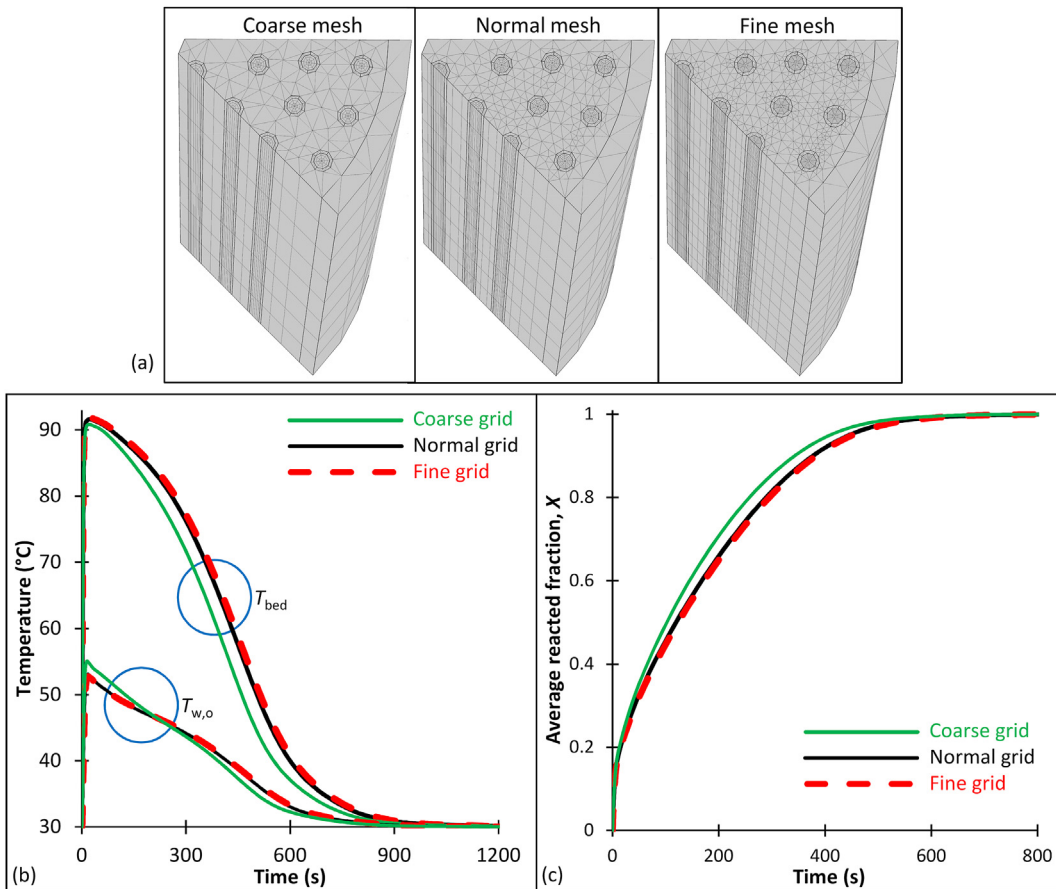


**Fig. 2 – (a) Meshing schemes, (b) and (c) grid independency tests with Shell141.3 mm-60Tubes design.**

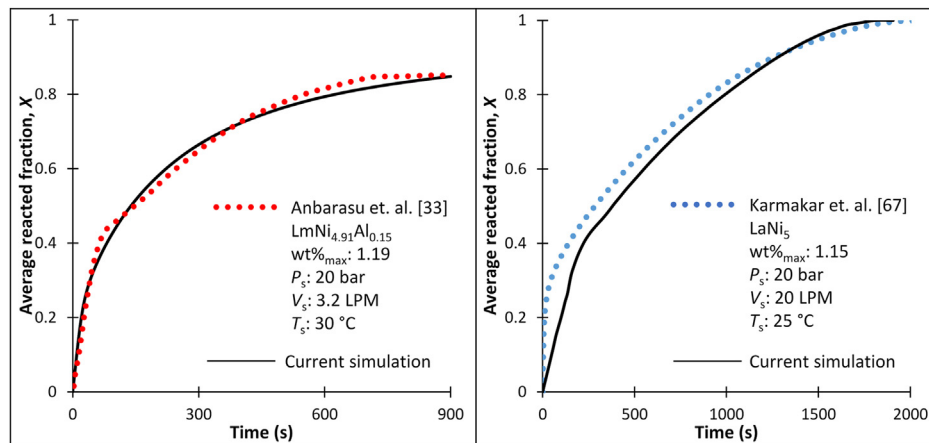


**Fig. 3 – Validation of the present numerical model with literature [33,67].**

Supplementary Information), viz.  $P_{\text{H}_2,\text{s}}/P_{\text{eq}}$ . The exothermic absorption generates heat throughout the MH bed, as a result of which  $P_{\text{eq}}$  rises. Thus, the  $P_{\text{H}_2,\text{s}}/P_{\text{eq}}$  ratio decreases leading to lowering of the driving force for hydrogen absorption. This slows down the absorption rate (Eq. S3 of in Supplementary Information) as seen in Fig. 4a. For example, the slope of  $X$  versus time curve decreases from  $X: \sim 0.15$  at  $\sim 10 \text{ s}$  when the average  $T_{\text{bed}}$  reaches peak value of  $\sim 92^\circ\text{C}$ . Fig. 4b shows the distribution snapshots of bed temperature and the

corresponding reacted fractions in the cross sections (at half-height) of the reactors at various time intervals of during hydrogen absorption. Fig. 4b also shows the hydrogen streamlines indicating the flow directions of hydrogen through the porous MH-bed. These streamline are estimated using Darcy's law (, Supplementary Information). This clearly shows that the presence of tubes does not restrict the hydrogen flow. The heat released during absorption is removed by water (HTF) flowing through the tubes (running

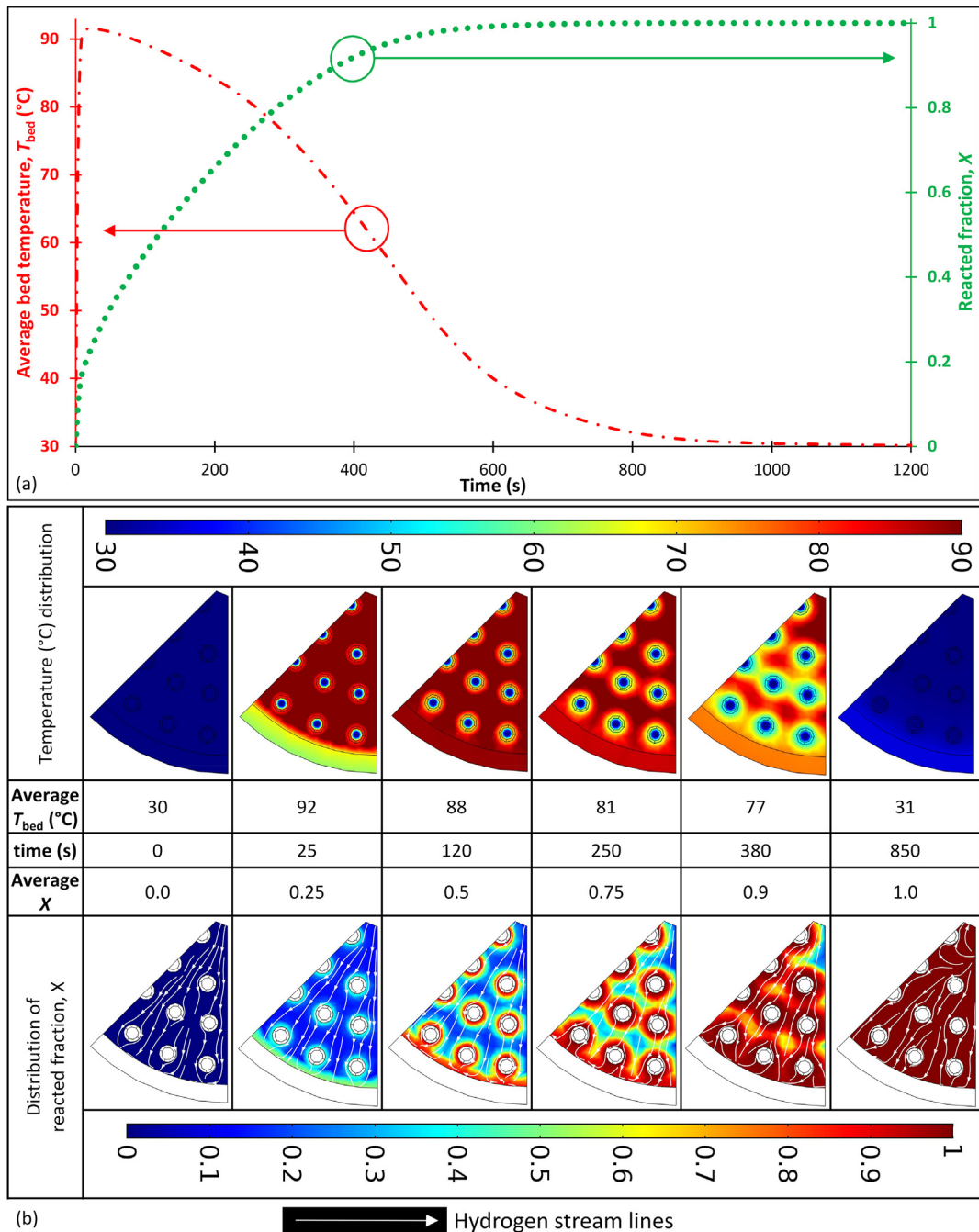


**Fig. 4 – (a) Time dependent variation of average  $T_{\text{bed}}$  and  $X$  of the design Shell141.3 mm-60Tubes; (b) distribution of temperature and  $X$  at various time instances along with hydrogen streamlines for a cut-plane situated at halfway along the height of Shell141.3 mm-60Tubes.**

perpendicular to the plane of these cross sections). From the distribution of  $T_{\text{bed}}$  and  $X$  in Fig. 4b, it is evident that after initial rise of temperature the region adjacent to the tube walls (circles in Fig. 4b) cools first. Further hydrogen absorption reaction occurs in these cold regions because of the reduced  $P_{\text{eq}}$  (i.e. high  $P_{\text{H}_2,\text{s}}/P_{\text{eq}}$ ) here. With time the colder region spreads away from the tube wall through the rest of the MH bed

leading to hydrogenation of these regions. The reaction ultimately stops due to overall saturation as the absorption rate is resisted by the reaction extent, expressed as  $(\rho_{\text{MH,sat}} - \rho_{\text{MH}})$  in Eq. S3 in Supplementary Information. This is visible at  $X \geq 0.9$  (Fig. 4a and b), where the reaction progression is slow despite lower  $T_{\text{bed}}$ . Beyond  $X: 0.9$  the  $X$  versus time curve almost saturates (Fig. 4a) and heat removal by water has little influence

on hydrogenation. Hence in the present study, the time required for 90% ( $X: 0.9$ ) hydrogen absorption is chosen for performance comparison.

#### 4.1. Comparison of performance between 1-pass-scheme and 4-pass-scheme

The 4-pass-scheme can provide four times higher water velocity ( $v_{w,4\text{-pass}}$ ) than that in 1-pass-scheme ( $v_{w,1\text{-pass}}$ ) at a fixed  $V_w$ , increasing the convective heat transfer coefficient. However, the inlet temperature ( $T_{w,i}$ ) in the latter passes of the 4-pass-scheme is more than that prior to the first pass, leading to a lower heat transfer capability. Hence, one of the objectives of the present work is to study the combined effect of these opposing conditions of higher water velocity and higher inlet temperature (particularly, in the latter passes). Such a combined effect decides the overall heat transfer and, eventually, the bed temperature and the duration of saturation.

A reactor shell of 141.3 mm OD with 60 tubes ( $n_{\text{tube}}$ , tubes arranged in 4 circular arrays, see Table 1) is used to study the effect of multiple passes in 4-pass-scheme. This design is

named Shell141.3 mm-60Tubes and the detailed design parameters can be found in Tables 1 and 2. In the 1-pass-scheme the total water flow rate,  $V_w: 10 \text{ LPM}$  gets divided into 60 equal parts as  $n_{\text{tube}}$ : 60 tubes are chosen. Thus, the velocity of water in each of the tubes is  $v_{w,1\text{-pass}}: 0.1692 \text{ m s}^{-1}$ . In the 4-pass-scheme, however, the same  $V_w: 10 \text{ LPM}$  is divided into  $n_{\text{tube}}/4$  i.e. 15 parts resulting in the water velocity of  $v_{w,4\text{-pass}}: 0.6667 \text{ m s}^{-1}$ . Fig. 5a shows the simulated results of the water inlet and outlet temperatures for every pass of the 4-pass-scheme as compared with those for the 1-pass-scheme. It should be noted that for the first passes of both these schemes the water inlet temperature is its supply temperature ( $T_{w,i}: 30^\circ\text{C}$ ). Also as mentioned above, the inlet temperature for any latter pass is equal to the outlet temperature of its previous pass (i.e.  $T_{w,i,n} = T_{w,o,n-1}$ ; where,  $n = 2$  to 4, Fig. 5a). For the latter passes (i.e.  $n = 2$  to 4) the inlet temperature of water increases steeply at the beginning, before decreasing gradually with time as seen in Fig. 5a. The initial rise in the water inlet temperature in the latter passes is a result of heat removal from their previous passes as shown in Fig. 5b. The difference in the inlet temperatures of any two subsequent

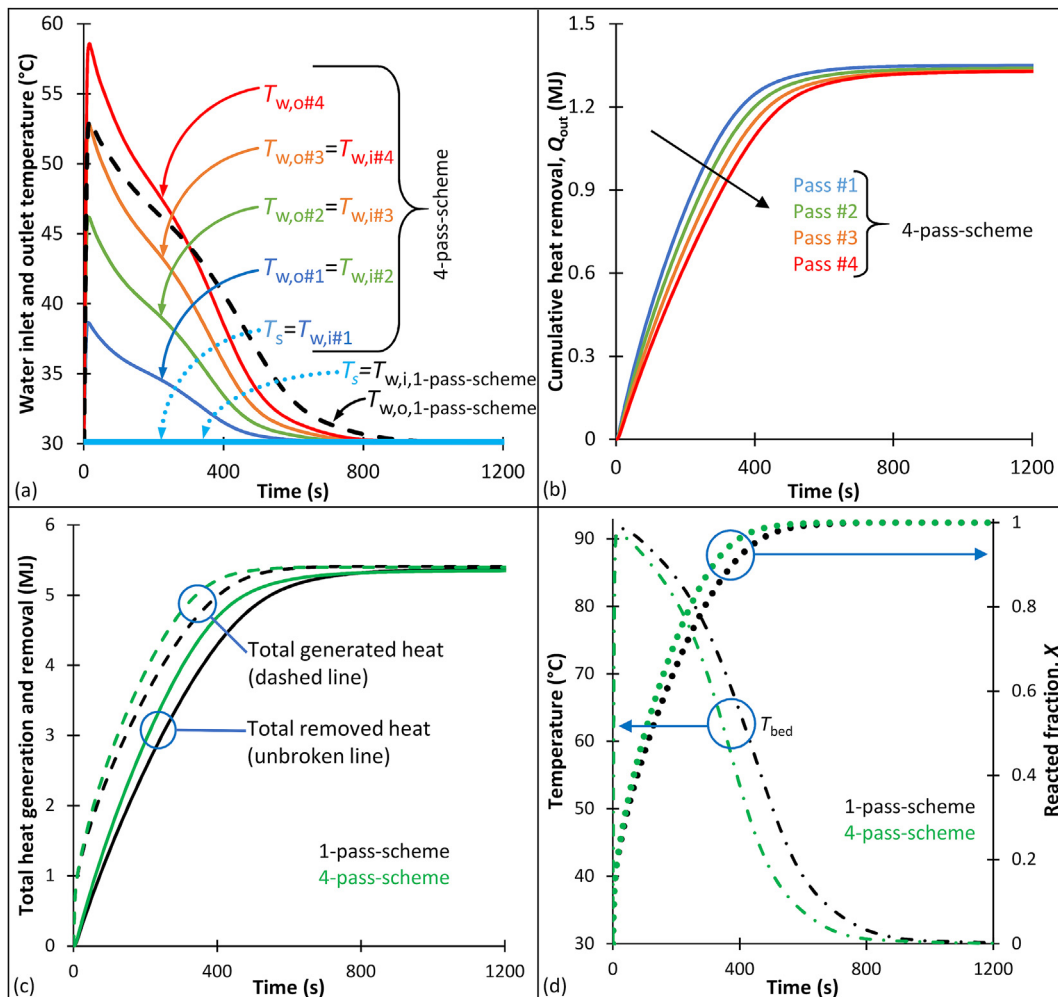


**Fig. 5 – Comparison between 1-pass-scheme and 4-pass-scheme with Shell141.3 mm-60Tubes design: (a) water inlet and outlet temperatures, (b) cumulative heat removal in each pass only in the 4-pass-scheme, (c) total heat generation and removal showing heat balance, and (d) temperature variation and extent of reaction with time.**

passes decreases with an increase in the number of passes (Fig. 5a). This is because of the lower heat removal from the previous passes as seen in Fig. 5b (indicated by arrow). From Fig. 5a the rise in the final water outlet temperature ( $T_{w,o\#4}$ ) of the 4-pass-scheme is higher than the corresponding rise in the 1-pass-scheme ( $T_{w,o, 1\text{-pass-scheme}}$ ). This is a result of the higher (rate of) heat removal in the 4-pass-scheme vis-à-vis that in the 1-pass-scheme. This is reflected in the steeper drop in the bed temperature ( $T_{\text{bed}}$ ) with time in the 4-pass-scheme as shown in Fig. 5d. Fig. 5d also shows that the reacted fraction reaches saturation in hydrogen absorption earlier in the 4-pass-scheme. For example, the duration for 90% saturation (i.e.  $X: 0.9$ , Fig. 5d) is 15.79% shorter in the 4-pass-scheme as opposed that in the 1-pass-scheme at  $P_{H_2,s}: 20$  bar,  $T_{w,i}: 30$  °C and  $V_w: 10$  LPM. Hence, to take advantage of the better performance, the rest of the studies are conducted considering 4-pass-scheme for water flow.

#### 4.2. Varying distance between tubes for a constant shell diameter

To study the effect of tube-spacing, i.e. distance between the adjacent water tubes on the hydrogen absorption performance, a reactor shell with a diameter of 141.3 mm (Sch-40s i.e. thickness of 6.55 mm) is chosen. For the present study, 3, 4 and 5 circular arrays of tubes are chosen as the designs, which are named as Shell141.3 mm-36Tubes, Shell141.3 mm-

60Tubes and Shell141.3 mm-92Tubes (Table 1). The designs with lower than 36 tubes are not considered as the tubes would be far apart and thus may not be effective in improving the performance. The designs with the number of tubes higher than 92 are also not considered due to the possible difficulties involved in the fabrication of reactors with such a number. The radial distance ( $p_r$ ) of these designs are calculated to be 19.35, 14.53 and 12.36 mm (Table 1), respectively. The height of the MH beds are chosen as 517, 553, and 610 mm to accommodate 25 kg LaNi<sub>5</sub> in all the reactors. Heat transfer improves with (i) higher water velocity ( $v_w$ ), (ii) higher total MH-tube contact surface area, and (iii) lower distance between the adjacent water tubes. The water velocity for a fixed  $V_w$  decreases with the increasing number of tubes. For Shell141.3 mm-36Tubes, Shell141.3 mm-60Tubes and Shell141.3 mm-92Tubes designs the calculated  $v_w$ s are 1.12, 0.68 and 0.44 m s<sup>-1</sup>, respectively. The lower the  $v_w$  the lower is the heat transfer. However, such a lowering of heat transfer is opposed by both the increased MH-tube contact surface area; and lower distance between the adjacent water tubes. The surface areas of Shell141.3 mm-36Tubes, Shell141.3 mm-60Tubes and Shell141.3 mm-92Tubes designs are 0.37, 0.66 and 1.12 m<sup>2</sup>, respectively. The combined effect of these three factors on the considered designs is shown in Fig. 6. Fig. 6a shows the  $T_{\text{bed}}$  and  $T_{w,o}$  versus time. A higher  $T_{w,o}$  indicates a higher rate of heat removal from the system under the same  $P_{H_2,s}$  and  $T_{w,i}$  conditions. The sudden rise in  $T_{w,o}$  indicates a

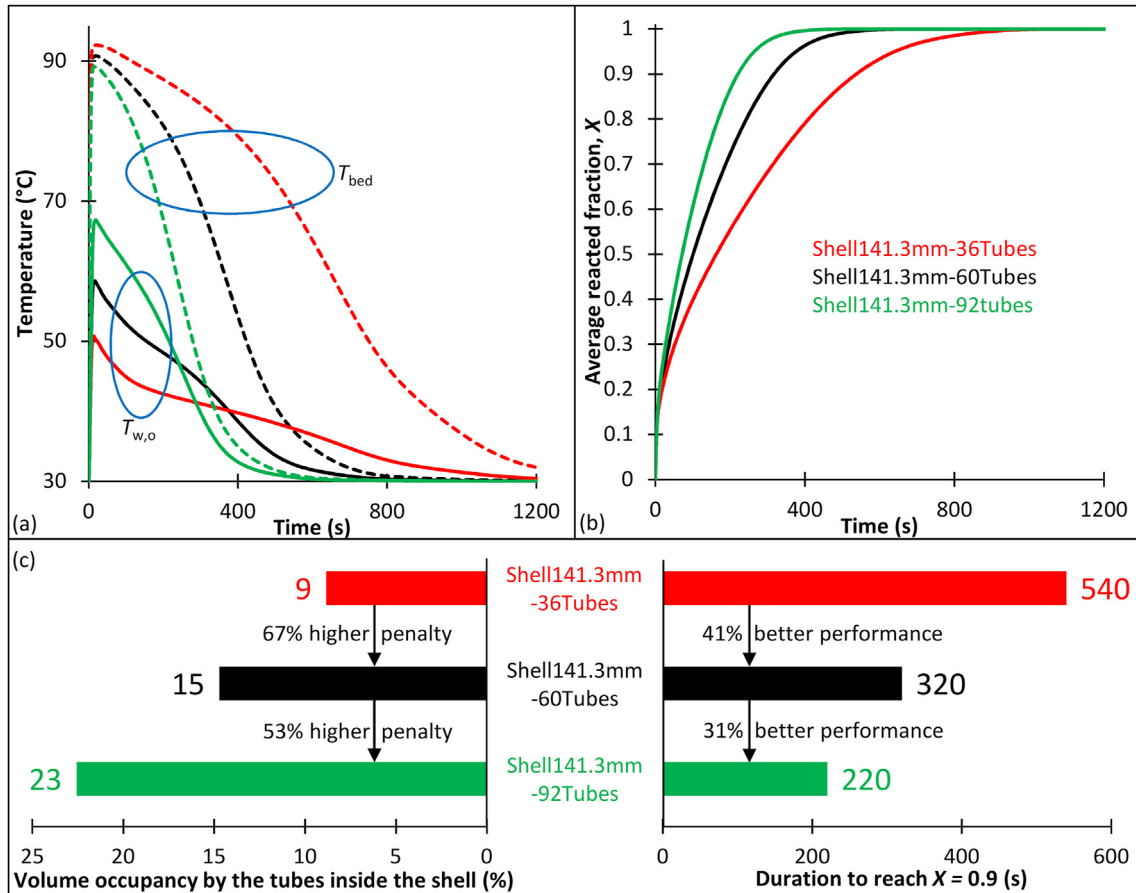


**Fig. 6 – Effect of varying distance between tubes for a constant shell diameter with 4-pass-scheme.**

quick absorption reaction followed by the heat transfer to the water. At this instance (20 s, Fig. 6a) of sudden rise in  $T_{w,o}$  its values are 50, 58 and 67 °C for 4-pass-scheme for Shell141.3 mm-36Tubes, Shell141.3 mm-60Tubes and Shell141.3 mm-92Tubes cases, respectively. Following this sudden rise, the  $T_{w,o}$  value is the highest for Shell141.3 mm-92Tubes design and the lowest in Shell141.3 mm-36Tubes design. Accordingly, the drop of  $T_{bed}$  is the steepest and gradual for these designs, respectively. These trends in  $T_{bed}$  and  $T_{w,o}$  clearly indicate the fastest and the slowest absorption reactions in Shell141.3 mm-92Tubes and Shell141.3 mm-36Tubes designs, respectively. These trends in progress of hydrogen absorption are shown through average reacted fraction ( $X$ ) in Fig. 6b. From Fig. 6a, after certain time, a reversal of the trend in  $T_{w,o}$  is observed with the lowest and the highest values in Shell141.3 mm-92Tubes and Shell141.3 mm-36Tubes designs, respectively, among all the designs. This is because, with the progress of time the highest (lowest) heat transfer occurs in Shell141.3 mm-92Tubes (Shell141.3 mm-36Tubes) design in the early stages of absorption, as mentioned above.

Fig. 5c and d shows the time required for 90% saturation ( $X: 0.9$ ) and HTS/MH volume ratio for the above-mentioned designs. The time required for  $X: 0.9$  reduces by ~40% from Shell141.3 mm-36Tubes (540 s) to Shell141.3 mm-60Tubes design (320 s); and by a further 31% from the latter to Shell141.3 mm-92Tubes design (220 s). As it is known, this reduction in time is equivalent to the improvement in performance by these percentage values. However, such a performance improvement comes at a cost of volumetric penalty as seen in Fig. 6d. For example, the HTS/MH volume ratio is the lowest for Shell141.3 mm-36Tubes design and the highest for Shell141.3 mm-92Tubes design. From this analysis, the Shell141.3 mm-60Tubes is a balanced design with a little trade-off between the time taken for saturation and HTS/MH volume ratio.

Shell141.3 mm-60Tubes has ~14 mm distance between the axes of two adjacent tubes, except for Array #1 (Table 1). The tubes are of 6.35 mm OD. Thus, tube-spacing (i.e. bed thickness between tubes) becomes ~7.6 mm. Interestingly, this lies between 5 and 10 mm which was suggested by other works as an optimal value [37]. Also, literature [33,37,60,70] shows the use of higher spacing between tubes closest to the central hydrogen filter and the current design does the same by allowing higher gaps of ~12 mm between the tubes of Array #1 (Table 1).

#### 4.3. Varying shell diameter for almost same distance between tubes

In our earlier study, we reported that the design with the shortest diameter offers the best performance for the same number of tubes considered in various designs [62]. However, as mentioned in our earlier study, it is difficult to fabricate such a design with the shortest diameter [62]. Hence, the objective is to study the effect of diameter, in other words the aspect ratio, on the performance by keeping the distance between the tubes almost the same. For this study, reactors with shell ODs of 114.3, 141.3, 168.3 mm (Sch-40s SS316 tubes) are considered with 36, 60 and 92 tubes arranged in 3, 4 and 5

circular arrays, respectively. Thus, making  $p_r$  (radial distance) almost the same for all these designs viz. 14–15 mm. These designs, are named as Shell114.3 mm-36Tubes, Shell141.3 mm-60Tubes, and Shell168.3 mm-92Tubes. In order to accommodate 25 kg LaNi<sub>5</sub>-bed in these designs the heights of 866, 553, and 386 mm are considered, respectively. Hence, the aspect ratios of these designs are ~7.6, ~3.9 and ~2.3, respectively. The detailed design parameters are furnished in Table 2. Such a significant difference in aspect ratio can affect the heat transfer. The other significant factor is  $v_w$  which has the values of 1.12, 0.68 and 0.44 m s<sup>-1</sup>, respectively, as mentioned above. The combined effect of all the design variations and velocities is represented in Fig. 7. From Fig. 7a the  $T_{w,o}$  curves as functions of time exhibit slight differences for all the designs. Such small differences in heat transfer are reflected in the  $T_{bed}$  curves (Fig. 7a) as well as in the average reacted fraction ( $X$ ) with time (Fig. 7b). The trends in  $T_{w,o}$  and  $T_{bed}$  are similar to those reported in the earlier section (see Section 4.2). Hence, they arise due to the similar reasons mentioned earlier.

The small differences in the performances of these designs are captured in Fig. 7a and b by showing the durations for 90% saturation ( $X: 0.9$ ) and HTS/MH volume ratio for these designs. The performance improvement in terms of reduction in duration for absorption are ~8.5% from Shell114.3 mm-36Tubes (350 s) to Shell141.3 mm-60Tubes (320 s). This improvement for Shell168.3 mm-92Tubes (305 s) design is ~4.7% over the Shell141.3 mm-60Tubes design. Such improvements, nevertheless, come with volumetric penalties through the HTS/MH ratios of 0.16, 0.17 and 0.19 in these designs, respectively. Hence, considering the trade-off between these performances and volumetric penalties Shell141.3 mm-60Tubes design offers an optimal solution for hydrogen storage.

The above analyses involving variations in the distance between the tubes (Section 4.2) and shell diameters (Section 4.3) suggests that the strategy to optimize the distance between the tubes is a more effective one for a given amount of MH weight.

## 5. Scaling up of the storage capacity by modular approach

Modular approach is chosen for scaling up of the storage capacity to 100 kg. Our earlier study [62] on systematic scaling up demonstrates that modular scale up by connecting multiple smaller reactors offers an improved performance over a single larger reactor for a given flow rate of heat transfer fluid. Moreover, the modular approach offers (i) convenience and flexibility in assembly and operation, (ii) reduced risk of an overall shut-down if any failure occurs, (iii) increasing capacity further by adding more modules. Hence, the optimized Shell141.3 mm-60Tubes reactor is chosen for scale-up to increase the total mass of LaNi<sub>5</sub> from 25 to 100 kg by connecting four such units in series and parallel through water tube connection. In series connection, named “4-Series”, the outlet water from a reactor would be the inlet for the next reactor. In parallel connection, named “4-Parallel”, the water flow gets divided into four equal parts before entering each of the

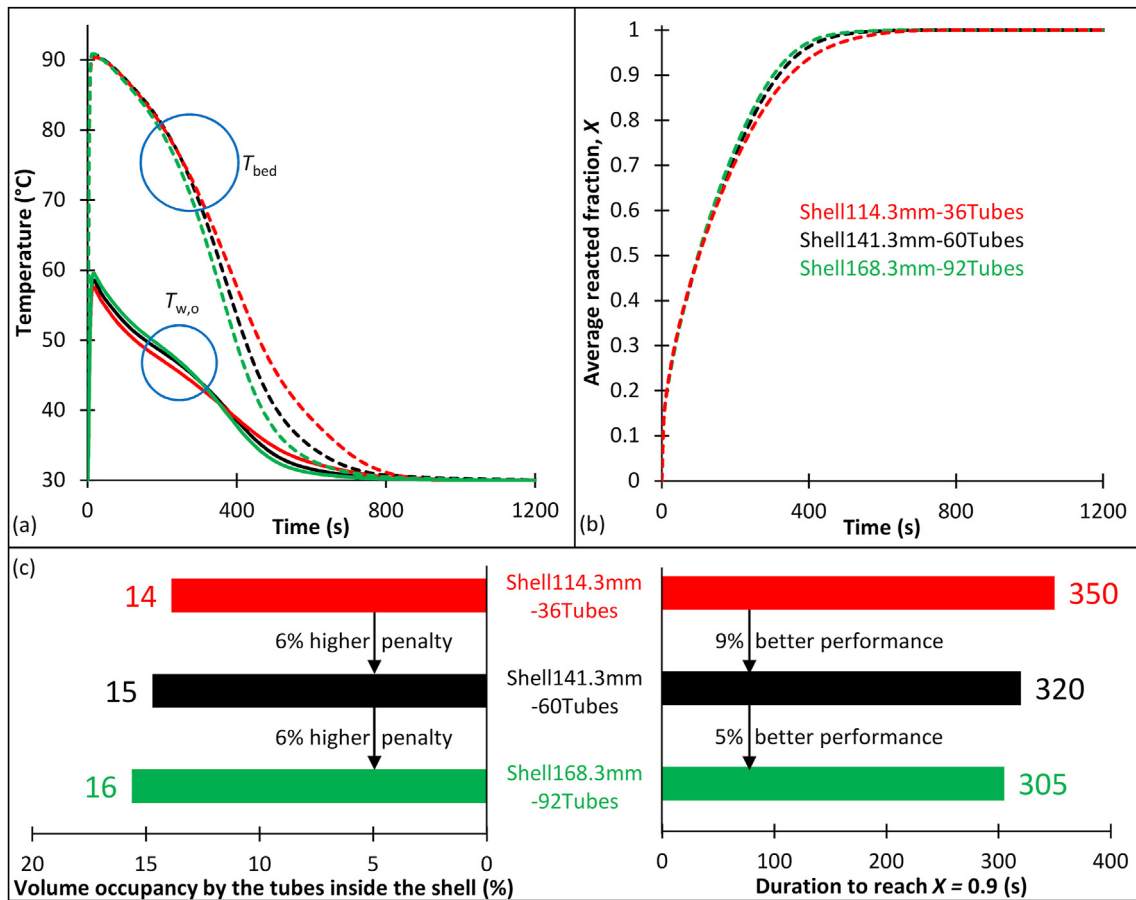


**Fig. 7 – Effect of varying shell diameter for almost same distance between tubes with 4-pass-scheme.**

reactors. The schematics of these configurations are shown in Fig. 8a and b.

For comparing the performance of the 4-Series and 4-Parallel configurations, the operating parameters are kept the same as before viz.  $P_{H2,s}$ : 20 bar,  $T_{w,i}$ : 30 °C. Two different water flow rates are considered viz.  $V_w$ : 10 and 40 LPM in separate cases. For the 4-Series configuration, it is assumed that the HTF (water) exits from a reactor and enters the next without losing any heat. Thus,  $T_{w,i,\text{Reactor}\#i+1} = T_{w,o,\text{Reactor}\#i}$  [ $i = 1$  to  $3$  for  $4$  reactors]. Since the water heats up before entering the latter reactors, it loses its cooling potential. Fig. 8c shows the  $T_{w,o}$ ,  $T_{bed}$  for all the four reactors (curves labeled as Reactor#1 to Reactor#4) at  $V_w$ : 10 LPM. Fig. 8c also shows the variation of these parameters for 4-Parallel configuration. Fig. 8d shows the variation of the average reacted fraction  $X$  for both 4-Series and 4-Parallel configurations at  $V_w$ : 10 LPM. These performance curves of Reactor#1 are the same as those shown in Fig. 5a and 6a (Shell141.3 mm-60Tubes). From Fig. 8c, the rise of temperature across the reactors gets lower for the latter reactors. This indicates poorer heat removal resulting from the higher water temperature in the latter reactors. The effect of this gradually decreased cooling effect is felt on the bed temperature ( $T_{bed}$ ). In other words,  $T_{bed}$  is higher for the latter reactors at any given time. This eventually leads to longer durations for reaction in those reactors (Fig. 8d). For

example, it takes 320, 425, 545 and 665 s to reach  $X: 0.9$  for Reactor#1, 2, 3 and 4, respectively. (Fig. 7b). In the case of 4-Parallel scheme, the total  $V_w$ : 10 LPM, gets divided into four equal parts and enters each of these four reactors. Hence, each of the four reactors receives 2.5 LPM of water flow rate entering at 30 °C. The cooling of the bed ( $T_{bed}$ , Fig. 8c) and subsequent absorption ( $X$ , Fig. 8d) happen simultaneously for all four reactors. It takes 625 s for 4-Parallel configuration to reach  $X: 0.9$ . The higher water velocity of 4-Series configuration helps Reactor#1, 2, and 3 to reach  $X: 0.9$  before the reactors in 4-Parallel one. However, Reactor#4 lags behind 4-Parallel due to the higher water temperature (Fig. 8d). The cause of poorer performance by the 4-Parallel is the lower (by 4 times) water flow rate in this configuration compared with that in the 4-Series configuration. The performance of the 4-Parallel configuration can be enhanced by increasing the flow rate into each of the reactors in this configuration.

For improving the performance of 4-Parallel configuration, water flow rate increased by four times to  $V_w$ : 40 LPM. Fig. 8e and f shows the  $T_{w,o}$ ,  $T_{bed}$  and  $X$ , respectively, for both 4-Series and 4-Parallel configurations at  $V_w$ : 40 LPM. In the 4-Parallel configuration, as mentioned earlier, the flow rate of water gets divided into four parts and enters each of the four reactors. Thus,  $V_w$ : 40 LPM in 4-Parallel configuration produces the same performance as a single reactor with  $V_w$ : 10 LPM (i.e.

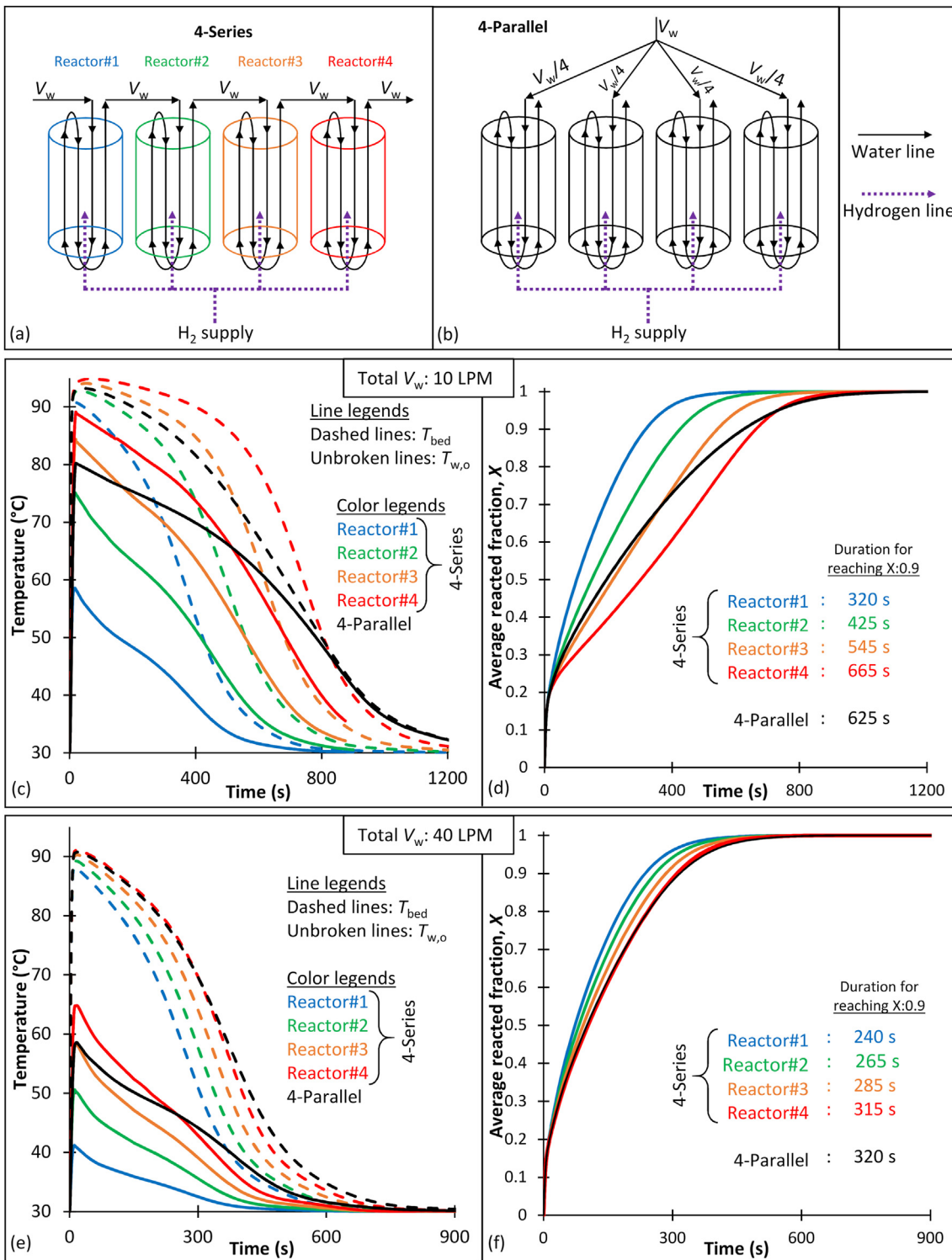


**Fig. 8 – Performance comparison between 4-Series and 4-Parallel configurations at 10 and 40 LPM of water flow.**

Shell141.3 mm-60Tubes in Figs. 5–7a and b). From Fig. 8f, at  $V_w$ : 40 LPM in the 4-Series configuration, Reactors #1–4 reach  $X: 0.9$  at ~240, 265, 285, and 315 s, respectively (Fig. 8f). Interestingly, all the four reactors of 4-Series reach  $X: 0.9$  before the

4-Parallel at  $V_w$ : 40 LPM (Fig. 8f). Nevertheless, the saturation times for series and parallel configurations are close to each other. Also from Fig. 8f, all the average reacted fraction curves are close to each other. This is mainly due to the chosen water

flow rate. This suggests that at higher flow rate the performances of both 4-Series and 4-Parallel configurations are almost similar.

As mentioned above, at lower flow rate of water ( $V_w$ : 10 LPM), first three reactors in 4-Series configuration individually offers better performance than the reactors in 4-Parallel. On the other hand, at higher flow rate of water ( $V_w$ : 40 LPM) all four reactors of 4-Series individually performs better than 4-Parallel but the difference in performance is much less significant. If average performance is considered, series configuration offers better performance at lower flow rate of water. Contrarily, either series or parallel can be used as per convenience at higher water flow rate.

## 6. Comparison of the performance with literature

The literature that used exact parameters as those used in the present study are almost non-existent. Hence new simulations were performed with the parameters similar to those used in literature to facilitate the comparison of the performances of the present reactor and those reported in literature. The optimized Shell141.3 mm-60Tubes reactor design from the present study was simulated with same  $P_{H2,s}$ ,  $T_{w,i}$  as reported in the literature and by proportionally changing  $V_w$ . The performance parameter for comparison is chosen as the duration for absorbing 1.2 wt% of hydrogen. Various metal hydride reactors have different maximum capacities and 1.2 wt% lies nearer to a 90% of their maximum capacity. The operating parameters along with the performance comparisons are summarised in Table 4.

Kumar et al. [36] used 99 cooling tubes and a single pass water flow through a 40 kg  $\text{LaNi}_{4.7}\text{Al}_{0.3}$  bed contained in a cylindrical shell. This material has a slightly lower but almost comparable plateau pressure as  $\text{LaNi}_5$  [71]. For the same  $P_{H2,s}$  and  $T_{w,i}$  and proportionally modified  $V_w$ , the present reactor performs similar to the one reported by Kumar et al. [36] for 1-pass-scheme. The reason for such similarity is the distance between tubes of the reactor in Ref. [36] and the present study are almost same. On the other hand, the utilization of 4-pass-scheme improves the performance significantly. This demonstrates the benefit of the multi pass scheme. In another work Prasad et al. [72] presented three reactor designs. Two without fins and one with fins. All have a central cooling channel along with a water jacket, creating an annulus of metal hydride ( $\text{LaNi}_5$ ) bed. Both unfinned designs contain 14.1 kg of  $\text{LaNi}_5$ . The present reactor performs significantly better than both of them (Table 4). But the finned design in Ref. [72] performs better than the present reactor. The presence of fins in Ref. [72] is responsible for such an improvement. However, it should be noted that with the presence of fins, there is a trade-off between storage capacity and space occupied by the heat transfer system. Hydrogen absorption by the reactor proposed by Jana et al. [73] lags behind significantly from the present reactor. This difference in the performance is despite their metal hydride viz.  $\text{La}_{0.8}\text{Ce}_{0.2}\text{Ni}_5$  possessing a higher and flatter plateau pressure [11]. Such a plateau renders only desorption easier. However, it suffers in absorption performance as can be seen from Table 4. The performance comparison clearly shows that

**Table 4 – Comparison of performance of the present design with literature.**

Literature	Reactor design approach	Mass (kg) and type of MH	$P_{H2,s}$ (bar)	$T_{w,i}$ (°C)	$V_w$ of literature (LPM)	$V_w$ used for comparison (LPM)	Time taken for absorbing 1.2 wt% of $\text{H}_2$ (s)	
							1-pass-scheme	4-pass-scheme
Present	Shell-and-tube	25 $\text{LaNi}_5$	20	30	10	250	340	280
Kumar et al. [36]	Shell-and-tube	40 $\text{LaNi}_{4.7}\text{Al}_{0.3}$	40	30	$\frac{30}{40} \cdot 25 = 18.75$	250	240	160
Prasad et al. [72]	Annular MH bed with central tube and water jacket (2 flow schemes) + flat circular fins	14.1 $\text{LaNi}_5$	15	25	$\frac{2.5}{14.1} \cdot 25 = 4.43$	500–550	485	420
Jana et al. [73]	19 Tubular MH tanks with common water jacket	26.5 $\text{La}_{0.8}\text{Ce}_{0.2}\text{Ni}_5$	20	20	25	$\frac{25}{26.5} \cdot 25 = 23.58$	800	235

the present optimized design can be always promising when 4-pass scheme is used.

The present work shows that multi pass scheme can be promising in the shell-tube type metal hydride reactors for hydrogen storage in modularly scaled up designs of up to at least 100 kg of metal hydride.

## 7. Conclusions

Hydrogen storage performance of a shell-and-tube type metal hydride reactor with 25 kg LaNi<sub>5</sub> is investigated. Multi pass scheme of heat transfer fluid (HTF) through the reactors is scarcely addressed in the context of hydrogen storage in literature. Hence, hydrogen storage performance of this type of reactors under multi pass scheme is investigated. Eventually, the modular scaling up of the optimum reactors to store 100 kg LaNi<sub>5</sub> is explored under multi pass scheme.

The cylindrical shell contains heat transfer tubes arranged in 3–5 circular arrays, which can facilitate four (multiple) passes of water as heat transfer fluid. The performance is compared between four and one passes (4-pass-scheme and 1-pass-scheme) for 20 bar H<sub>2</sub> supply pressure (P<sub>H<sub>2</sub>,s</sub>), total water volume flow rate (V<sub>w</sub>) of 10 LPM and 30 °C water inlet temperature (T<sub>w,i</sub>). The time taken for 90% of the maximum theoretical hydrogen storage capacity of 25 kg LaNi<sub>5</sub> is chosen as the parameter on which the performance is evaluated. Scale up of this reactor is studied for its performance by connecting four such 25 kg reactor modules with 4-pass-scheme in series and parallel configurations to store 100 kg LaNi<sub>5</sub>. The following are the important conclusions of the present study.

- The design of a reactor is driven by a trade-off between the volume occupied by the tubes inside the shell and the enhanced absorption performance due to higher number of tubes. To find a balance between these factors, commercially available SS316 standard shell (Sch-40s) with outer diameter [OD] of 141.3 was chosen with 36, 60 and 92 tubes arranged in 3, 4 and 5 circular arrays, separately. The 60 tubes arranged in 4 circular arrays was a balanced arrangement (design) for the aforementioned shell OD.
- Identifying the optimum shell OD, while keeping the center-to-center tube distance almost similar, is conducted using 36, 60 and 92 tubes arranged in 3, 4 and 5 circular arrays inside shells. For this purpose, commercial SS316 shells of 114.3, 141.3 and 168.3 mm ODs are used. The results suggest that the configuration consisting of the shell with 141.3 mm OD and 60 tubes arranged in 4 circular arrays (Shell141.3 mm-60Tubes) offers the optimum capacity and absorption performance.
- The performance of this optimum Shell141.3 mm-60Tubes design improves by ~15.79% when using 4-pass-scheme over 1-pass-scheme, due to four times higher water velocity in the former.
- For scale up, four optimum Shell141.3 mm-60Tubes modular reactors with 4-pass-scheme are used in series and parallel configurations through water tubing connection. At lower water flow rate (V<sub>w</sub>) of 10 LPM the series configuration results in an overall faster absorption reaction. When V<sub>w</sub> is increased to 40 LPM the series and parallel

configurations perform similarly. This offers a convenient choice between these configurations for implementation.

## Declaration of competing interest

The authors declare that they have no known competing financial interests or personal relationships that could have appeared to influence the work reported in this paper.

## Appendix A. Supplementary data

Supplementary data to this article can be found online at <https://doi.org/10.1016/j.ijhydene.2023.09.128>.

## R E F E R E N C E S

- [1] Gupta RB. Hydrogen fuel: production, transport, and storage. CRC Press; 2008.
- [2] Ahmad H, Kamarudin SK, Minggu LJ, Kassim M. Hydrogen from photo-catalytic water splitting process: a review. Renew Sustain Energy Rev 2015;43:599–610. <https://doi.org/10.1016/j.rser.2014.10.101>.
- [3] Tanksale A, Beltramini JN, Lu GQM. A review of catalytic hydrogen production processes from biomass. Renew Sustain Energy Rev 2010;14:166–82. <https://doi.org/10.1016/j.rser.2009.08.010>.
- [4] Kurnia JC, Sasmito AP, Shamim T. Advances in proton exchange membrane fuel cell with dead-end anode operation: a review. Appl Energy 2019;252:113416. <https://doi.org/10.1016/j.apenergy.2019.113416>.
- [5] Lin RH, Xi XN, Wang PN, Wu BD, Tian SM. Review on hydrogen fuel cell condition monitoring and prediction methods. Int J Hydrogen Energy 2019;44:5488–98. <https://doi.org/10.1016/j.ijhydene.2018.09.085>.
- [6] Peighambardoust SJ, Rowshanzamir S, Amjadi M. Review of the proton exchange membranes for fuel cell applications. Int J Hydrogen Energy 2010;35:9349–84. <https://doi.org/10.1016/j.ijhydene.2010.05.017>.
- [7] Gurz M, Baltacioglu E, Hames Y, Kaya K. The meeting of hydrogen and automotive: a review. Int J Hydrogen Energy 2017;42:23334–46. <https://doi.org/10.1016/j.ijhydene.2017.02.124>.
- [8] Dimitriou P, Tsujimura T. A review of hydrogen as a compression ignition engine fuel. Int J Hydrogen Energy 2017;42:24470–86. <https://doi.org/10.1016/j.ijhydene.2017.07.232>.
- [9] Verhelst S. Recent progress in the use of hydrogen as a fuel for internal combustion engines. Int J Hydrogen Energy 2014;39:1071–85. <https://doi.org/10.1016/j.ijhydene.2013.10.102>.
- [10] Liang G, Huot J, Schulz R. Hydrogen storage properties of the mechanically alloyed LaNi<sub>5</sub>-based materials. J Alloys Compd 2001;320:133–9. [https://doi.org/10.1016/S0925-8388\(01\)00929-X](https://doi.org/10.1016/S0925-8388(01)00929-X).
- [11] Odysseos M, De Rango P, Christodoulou CN, Hlil EK, Steriotis T, Karagiorgis G, et al. The effect of compositional changes on the structural and hydrogen storage properties of (La-Ce)Ni<sub>5</sub>type intermetallics towards compounds suitable for metal hydride hydrogen compression. J Alloys Compd 2013;580:S268–70. <https://doi.org/10.1016/j.jallcom.2013.01.057>.

- [12] Liu J, Li K, Cheng H, Yan K, Wang Y, Liu Y, et al. New insights into the hydrogen storage performance degradation and Al functioning mechanism of LaNi<sub>5-x</sub>Al<sub>x</sub>alloys. *Int J Hydrogen Energy* 2017;42:24904–14. <https://doi.org/10.1016/j.ijhydene.2017.07.213>.
- [13] Liu G, Chen D, Wang Y, Yang K. Experimental and computational investigations of LaNi<sub>5-x</sub>Al<sub>x</sub> (x = 0, 0.25, 0.5, 0.75 and 1.0) tritium-storage alloys. *J Mater Sci Technol* 2018;34:1699–712. <https://doi.org/10.1016/j.jmst.2018.01.007>.
- [14] Oliva DG, Fuentes M, Borzone EM, Meyer GO, Aguirre PA. Hydrogen storage on LaNi<sub>5-x</sub>Sn<sub>x</sub>. Experimental and phenomenological Model-based analysis. *Energy Convers Manag* 2018;173:113–22. <https://doi.org/10.1016/j.enconman.2018.07.041>.
- [15] Spodryk M, Gasilova N, Züttel A. Hydrogen storage and electrochemical properties of LaNi<sub>5-x</sub>Cu<sub>x</sub> hydride-forming alloys. *J Alloys Compd* 2019;775:175–80. <https://doi.org/10.1016/j.jallcom.2018.10.009>.
- [16] Endo N, Suzuki S, Goshoma K, Maeda T. Operation of a bench-scale TiFe-based alloy tank under mild conditions for low-cost stationary hydrogen storage. *Int J Hydrogen Energy* 2017;42:5246–51. <https://doi.org/10.1016/j.ijhydene.2016.11.088>.
- [17] Ma J, Pan H, Wang X, Chen C, Wang Q. Hydrogen storage properties of FeTi<sub>1.3+x</sub> wt%Mm (x=0.0, 1.5, 3.0, 4.5, 6.0) hydrogen storage alloys. *Int J Hydrogen Energy* 2000;25:779–82. [https://doi.org/10.1016/S0360-3199\(99\)00100-7](https://doi.org/10.1016/S0360-3199(99)00100-7).
- [18] Qu H, Du J, Pu C, Niu Y, Huang T, Li Z, et al. Effects of Co introduction on hydrogen storage properties of Ti-Fe-Mn alloys. *Int J Hydrogen Energy* 2015;40:2729–35. <https://doi.org/10.1016/j.ijhydene.2014.12.089>.
- [19] Shrinivasan S, Goswami H, Tien HY, Tanniru M, Ebrahimi F, Tatiparti SSV. Contributions of multiple phenomena towards hydrogenation: a case of Mg. *Int J Hydrogen Energy* 2015;40:13518–29. <https://doi.org/10.1016/j.ijhydene.2015.08.018>.
- [20] Au M. Hydrogen storage properties of magnesium based nanostructured composite materials. *Mater Sci Eng B Solid-State Mater Adv Technol* 2005;117:37–44. <https://doi.org/10.1016/j.mseb.2004.10.017>.
- [21] Imamura H, Kitazawa I, Tanabe Y, Sakata Y. Hydrogen storage in carbon/Mg nanocomposites synthesized by ball milling. *Int J Hydrogen Energy* 2007;32:2408–11. <https://doi.org/10.1016/j.ijhydene.2006.10.058>.
- [22] Jain IP, Lal C, Jain A. Hydrogen storage in Mg: a most promising material. *Int J Hydrogen Energy* 2010;35:5133–44. <https://doi.org/10.1016/j.ijhydene.2009.08.088>.
- [23] Sakintuna B, Lamari-Darkrim F, Hirscher M. Metal hydride materials for solid hydrogen storage: a review. *Int J Hydrogen Energy* 2007;32:1121–40. <https://doi.org/10.1016/j.ijhydene.2006.11.022>.
- [24] Srinivasa Murthy S. Heat and mass transfer in solid state hydrogen storage: a review. *J Heat Tran* 2012;134:1–11. <https://doi.org/10.1115/1.4005156>.
- [25] Askri F, Ben Salah M, Jemni A, Ben Nasrallah S. Optimization of hydrogen storage in metal-hydride tanks. *Int J Hydrogen Energy* 2009;34:897–905. <https://doi.org/10.1016/j.ijhydene.2008.11.021>.
- [26] Kaplan Y. Effect of design parameters on enhancement of hydrogen charging in metal hydride reactors. *Int J Hydrogen Energy* 2009;34:2288–94. <https://doi.org/10.1016/j.ijhydene.2008.12.096>.
- [27] El Mghari H, Huot J, Xiao J. Analysis of hydrogen storage performance of metal hydride reactor with phase change materials. *Int J Hydrogen Energy* 2019;44:28893–908. <https://doi.org/10.1016/j.ijhydene.2019.09.090>.
- [28] Arslan B, Ilbas M, Celik S. Experimental analysis of hydrogen storage performance of a LaNi<sub>5</sub>–H<sub>2</sub> reactor with phase change materials. *Int J Hydrogen Energy* 2023;48:6010–22. <https://doi.org/10.1016/j.ijhydene.2022.11.083>.
- [29] Hassan IA, Mohammed RH, Ramadan HS, Saleh MA, Cuevas F, Hissel D. Performance evaluation of a novel concentric metal hydride reactor assisted with phase change material. *Appl Therm Eng* 2023;224:120065. <https://doi.org/10.1016/j.applthermaleng.2023.120065>.
- [30] Ye Y, Lu J, Ding J, Wang W, Yan J. Numerical simulation on the storage performance of a phase change materials based metal hydride hydrogen storage tank. *Appl Energy* 2020;278:115682. <https://doi.org/10.1016/j.apenergy.2020.115682>.
- [31] Lutz M, Bhouri M, Linder M, Bürger I. Adiabatic magnesium hydride system for hydrogen storage based on thermochemical heat storage: numerical analysis of the dehydrogenation. *Appl Energy* 2019;236:1034–48. <https://doi.org/10.1016/j.apenergy.2018.12.038>.
- [32] Muthukumar P, Singhal A, Bansal GK. Thermal modeling and performance analysis of industrial-scale metal hydride based hydrogen storage container. *Int J Hydrogen Energy* 2012;37:14351–64. <https://doi.org/10.1016/j.ijhydene.2012.07.010>.
- [33] Anbarasu S, Muthukumar P, Mishra SC. Tests on MnNi<sub>4.91</sub>Sn<sub>0.15</sub> based solid state hydrogen storage device with embedded cooling tubes - Part A: absorption process. *Int J Hydrogen Energy* 2014;39:3342–51. <https://doi.org/10.1016/j.ijhydene.2013.12.090>.
- [34] Raju NN, Kumar A, Malleswararao K, Muthukumar P. Parametric studies on LaNi<sub>4.7</sub>Al<sub>0.3</sub> based hydrogen storage reactor with embedded cooling tubes. *Energy Proc* 2019;158:2384–90. <https://doi.org/10.1016/j.egypro.2019.01.288>.
- [35] Kumar A, Raju NN, Muthukumar P. Parametric studies on MnNi<sub>4.7</sub>Fe<sub>0.3</sub> based reactor with embedded cooling tubes for hydrogen storage and cooling application. *J Energy Storage* 2021;35:102317. <https://doi.org/10.1016/j.est.2021.102317>.
- [36] Kumar A, Raju NN, Muthukumar P, Selvan PV. Experimental studies on industrial scale metal hydride based hydrogen storage system with embedded cooling tubes. *Int J Hydrogen Energy* 2019;44:13549–60. <https://doi.org/10.1016/j.ijhydene.2019.03.180>.
- [37] Raju NN, Muthukumar P, Selvan PV, Malleswararao K. Design methodology and thermal modelling of industrial scale reactor for solid state hydrogen storage. *Int J Hydrogen Energy* 2019;44:20278–92. <https://doi.org/10.1016/j.ijhydene.2019.05.193>.
- [38] Gkanas EI, Khzouz M, Panagakos G, Statheros T, Mihalakakou G, Siasos GI, et al. Hydrogenation behavior in rectangular metal hydride tanks under effective heat management processes for green building applications. *Energy* 2018;142:518–30. <https://doi.org/10.1016/j.energy.2017.10.040>.
- [39] Liu Y, Ayub I, Khan MR, Yang F, Wu Z, Zhang Z. Numerical investigation of metal hydride heat storage reactor with two types multiple heat transfer tubes structures. *Energy* 2022;253:124142. <https://doi.org/10.1016/j.energy.2022.124142>.
- [40] Pandey V, Krishna KV, Maiya MP. Numerical modelling and heat transfer optimization of large-scale multi-tubular metal hydride reactors. *Int J Hydrogen Energy* 2023;48:16020–36. <https://doi.org/10.1016/j.ijhydene.2023.01.058>.
- [41] Afzal M, Sharma N, Gupta N, Sharma P. Transient simulation studies on a metal hydride based hydrogen storage reactor with longitudinal fins. *J Energy Storage* 2022;51:104426. <https://doi.org/10.1016/j.est.2022.104426>.

- [42] Gupta N, Tiwari S, Nitin, Khandarkar RJ, Afzal M, Sharma P. Experimental studies on novel multi tubular reactor with shell having integrated buffer storage. *J Energy Storage* 2023;67:107491. <https://doi.org/10.1016/j.est.2023.107491>.
- [43] Aadithiyian AK, Seeraj R, Anbarasu S. Thermal modelling and performance evaluation of  $\text{LmNi}_{4.91}\text{Sn}_{0.15}$  hydride bed configurations for space-constrained thermal applications. *Appl Therm Eng* 2022;216:119116. <https://doi.org/10.1016/j.applthermaleng.2022.119116>.
- [44] Seeraj R, Aadithiyian AK, Anbarasu S. Comparison, advancement, and performance evaluation of heat exchanger assembly in solid-state hydrogen storage device. *Renew Energy* 2022;198:667–78. <https://doi.org/10.1016/j.renene.2022.08.051>.
- [45] Bai XS, Yang WW, Tang XY, Yang FS, Jiao YH, Yang Y. Optimization of tree-shaped fin structures towards enhanced absorption performance of metal hydride hydrogen storage device: a numerical study. *Energy* 2021;220:119738. <https://doi.org/10.1016/j.energy.2020.119738>.
- [46] Krishna KV, Pandey V, Maiya MP. Bio-inspired leaf-vein type fins for performance enhancement of metal hydride reactors. *Int J Hydrogen Energy* 2022;47:23694–709. <https://doi.org/10.1016/j.ijhydene.2022.05.163>.
- [47] Lesmana LA, Lu C, Chen F, Aziz M. Triply periodic minimal surface gyroid structure as effective metal hydride hydrogen storage reactor: experimental study. *Therm Sci Eng Prog* 2023;42:101903. <https://doi.org/10.1016/j.tsep.2023.101903>.
- [48] Chang H, Tao YB, Wang WY. Numerical study on storage performance of metal hydride reactors with multiple spiral fins. *Int J Hydrogen Energy* 2023. <https://doi.org/10.1016/j.ijhydene.2023.05.248>.
- [49] Bai XS, Yang WW, Tang XY, Yang FS, Jiao YH, Yang Y. Hydrogen absorption performance investigation of a cylindrical MH reactor with rectangle heat exchange channels. *Energy* 2021;232:121101. <https://doi.org/10.1016/j.energy.2021.121101>.
- [50] Eisapour AH, Naghizadeh A, Eisapour M, Talebizadehsardari P. Optimal design of a metal hydride hydrogen storage bed using a helical coil heat exchanger along with a central return tube during the absorption process. *Int J Hydrogen Energy* 2021;46:14478–93. <https://doi.org/10.1016/j.ijhydene.2021.01.170>.
- [51] Tiwari S, Sharma P. Optimization based methodology to design metal hydride reactor for thermal storage application. *J Energy Storage* 2021;41:102845. <https://doi.org/10.1016/j.est.2021.102845>.
- [52] Bao Z, Mou X. Experimental study on temperature variation of metal hydride reactor incorporating helically coiled heat exchanger during absorption. *J Energy Storage* 2021;44:103438. <https://doi.org/10.1016/j.est.2021.103438>.
- [53] Wang D, Li S, Huang Z, Liu Z, Wang Y, Yang F, et al. Design optimization, sensitivity analysis and operational comparison of a duplex helical elliptical tube metal hydride reactor. *Sustain Energy Fuels* 2020;4:5851–68. <https://doi.org/10.1039/dose01028f>.
- [54] Wang D, Wang Y, Wang F, Zheng S, Guan S, Zheng L, et al. Hydrogen storage in branch mini-channel metal hydride reactor: optimization design, sensitivity analysis and quadratic regression. *Int J Hydrogen Energy* 2021;46:25189–207. <https://doi.org/10.1016/j.ijhydene.2021.05.051>.
- [55] Singh A, Maiya MP, Srinivasa Murthy S. Experiments on solid state hydrogen storage device with a finned tube heat exchanger. *Int J Hydrogen Energy* 2017;42:15226–35. <https://doi.org/10.1016/j.ijhydene.2017.05.002>.
- [56] Singh A, Prakash Maiya M, Srinivasa Murthy S. Performance of a solid state hydrogen storage device with finned tube heat exchanger. *Int J Hydrogen Energy* 2017;42:26855–71. <https://doi.org/10.1016/j.ijhydene.2017.06.071>.
- [57] Lewis SD, Chippipar P, Deb A. Numerical study of hydrogen absorption in a metal hydride tank embedded with multiple U-shaped cooling channel. *AIP Conf Proc* 2020;2236:1–8. <https://doi.org/10.1063/5.0006858>. 030004.
- [58] Visaria M, Mudawar I, Pourpoint T. Enhanced heat exchanger design for hydrogen storage using high-pressure metal hydride: Part 1. Design methodology and computational results. *Int J Heat Mass Tran* 2011;54:413–23. <https://doi.org/10.1016/j.ijheatmasstransfer.2010.09.029>.
- [59] Visaria M, Mudawar I, Pourpoint T. Enhanced heat exchanger design for hydrogen storage using high-pressure metal hydride - Part 2. Experimental results. *Int J Heat Mass Tran* 2011;54:424–32. <https://doi.org/10.1016/j.ijheatmasstransfer.2010.09.028>.
- [60] Anbarasu S, Muthukumar P, Mishra SC. Thermal modeling of  $\text{LmNi}_{4.91}\text{Sn}_{0.15}$  based solid state hydrogen storage device with embedded cooling tubes. *Int J Hydrogen Energy* 2014;39:15549–62. <https://doi.org/10.1016/j.ijhydene.2014.07.088>.
- [61] Chandra S, Sharma P, Muthukumar P, Tatiparti SSV. Modeling and numerical simulation of a 5 kg  $\text{LaNi}_5$ -based hydrogen storage reactor with internal conical fins. *Int J Hydrogen Energy* 2020;45:8794–809. <https://doi.org/10.1016/j.ijhydene.2020.01.115>.
- [62] Chandra S, Sharma P, Muthukumar P, Tatiparti SSV. Strategies for scaling-up  $\text{LaNi}_5$ -based hydrogen storage system with internal conical fins and cooling tubes. *Int J Hydrogen Energy* 2021;46:19031–45. <https://doi.org/10.1016/j.ijhydene.2021.03.056>.
- [63] Chandra S, Sharma P, Muthukumar P, Tatiparti SSV. Experimental hydrogen sorption study on a  $\text{LaNi}_5$ -based 5 kg reactor with novel conical fins and water tubes and its numerical scale-up through a modular approach. *Int J Hydrogen Energy* 2022. <https://doi.org/10.1016/j.ijhydene.2022.08.098>.
- [64] Mellouli S, Askri F, Dhaou H, Jemni A, Ben Nasrallah S. Numerical simulation of heat and mass transfer in metal hydride hydrogen storage tanks for fuel cell vehicles. *Int J Hydrogen Energy* 2010;35:1693–705. <https://doi.org/10.1016/j.ijhydene.2009.12.052>.
- [65] Singh A, Maiya MP, Murthy SS. Effects of heat exchanger design on the performance of a solid state hydrogen storage device. *Int J Hydrogen Energy* 2015;40:9733–46. <https://doi.org/10.1016/j.ijhydene.2015.06.015>.
- [66] Busqué R, Torres R, Grau J, Roda V, Husar A. Effect of metal hydride properties in hydrogen absorption through 2D-axisymmetric modeling and experimental testing in storage canisters. *Int J Hydrogen Energy* 2017;42:19114–25. <https://doi.org/10.1016/j.ijhydene.2017.06.125>.
- [67] Karmakar A, Mallik A, Gupta N, Sharma P. Studies on 10 kg alloy mass metal hydride based reactor for hydrogen storage. *Int J Hydrogen Energy* 2021;46:5495–506. <https://doi.org/10.1016/j.ijhydene.2020.11.091>.
- [68] Gkanas EI, Grant DM, Khzouz M, Stuart AD, Manickam K, Walker GS. Efficient hydrogen storage in up-scale metal hydride tanks as possible metal hydride compression agents equipped with aluminium extended surfaces. *Int J Hydrogen Energy* 2016;41:10795–810. <https://doi.org/10.1016/j.ijhydene.2016.04.035>.
- [69] Wang D, Wang Y, Huang Z, Yang F, Wu Z, Zheng L, et al. Design optimization and sensitivity analysis of the radiation mini-channel metal hydride reactor. *Energy* 2019;173:443–56. <https://doi.org/10.1016/j.energy.2019.02.033>.
- [70] Anbarasu S, Muthukumar P, Mishra SC. Tests on  $\text{LmNi}_{4.91}\text{Sn}_{0.15}$  based solid state hydrogen storage device with

- embedded cooling tubes - Part B: desorption process. Int J Hydrogen Energy 2014;39:4966–72. <https://doi.org/10.1016/j.ijhydene.2014.01.039>.
- [71] Liu J, Li K, Cheng H, Yan K, Wang Y, Liu Y, et al. New insights into the hydrogen storage performance degradation and Al functioning mechanism of  $\text{LaNi}_{5-x}\text{Al}_x$  alloys. Int J Hydrogen Energy 2017;42:24904–14. <https://doi.org/10.1016/j.ijhydene.2017.07.213>.
- [72] Sunku Prasad J, Muthukumar P. Design and performance analysis of an annular metal hydride reactor for large-scale hydrogen storage applications. Renew Energy 2022;181:1155–66. <https://doi.org/10.1016/j.renene.2021.09.109>.
- [73] Jana S, Muthukumar P. Design, development and hydrogen storage performance testing of a tube bundle metal hydride reactor. J Energy Storage 2023;63:106936. <https://doi.org/10.1016/j.est.2023.106936>.
- [74] Boukhari A, Bessaïh R. Numerical heat and mass transfer investigation of hydrogen absorption in an annulus-disc reactor. Int J Hydrogen Energy 2015;40:13708–17. <https://doi.org/10.1016/j.ijhydene.2015.05.123>.
- [75] Chibani A, Bougriou C. Effect of the tank geometry on the storage and destocking of hydrogen on metal hydride ( $\text{LaNi}_5-\text{H}_2$ ). Int J Hydrogen Energy 2017;42:23035–44. <https://doi.org/10.1016/j.ijhydene.2017.07.102>.